J. Fluid Mech. (1991), *vol.* 231, *pp.* 257–301
Printed in Great Britain

Evolution of streamwise vortices and generation of small-scale motion in a plane mixing layer

By K. J. NYGAARD AND A. GLEZER
Department of Aerospace and Mechanical Engineering, The University of Arizona, Tucson, AZ 85721, USA

(Received 26 July 1990 and in revised form 21 March 1991)

The evolution of streamwise vortices in a plane mixing layer and their role in the generation of small-scale three-dimensional motion are studied in a closed-return water facility. Spanwise-periodic streamwise vortices are excited by a time-harmonic wavetrain with spanwise-periodic amplitude variations synthesized by a mosaic of 32 surface film heaters flush-mounted on the flow partition. For a given excitation frequency, virtually any spanwise wavelength synthesizable by the heating mosaic can be excited and can lead to the formation of streamwise vortices before the rollup of the primary vortices is completed. The onset of streamwise vortices is accompanied by significant distortion in the transverse distribution of the streamwise velocity component. The presence of inflexion points, absent in corresponding velocity distributions of the unforced flow, suggests the formation of locally unstable regions of large shear in which broadband perturbations already present in the base flow undergo rapid amplification, followed by breakdown to small-scale motion. Furthermore, as a result of spanwise-non-uniform excitation the cores of the primary vortices are significantly altered. The three-dimensional features of the streamwise vortices and their interaction with the base flow are inferred from surfaces of r.m.s. velocity fluctuations and an approximation to cross-stream vorticity using three-dimensional single component velocity data. The striking enhancement of small-scale motion and the spatial modification of its distribution, both induced by the streamwise vortices, can be related to the onset of the mixing transition.

1. Introduction

The rate at which a reaction product is formed in the mixing layer between two reacting streams can increase by an order of magnitude through a mixing transition downstream of the flow partition (Roshko 1981). The small-scale three-dimensional motion necessary for such mixing enhancement has been connected by Roshko to the appearance of streamwise counter-rotating vortex pairs first observed by Miksad (1972) and Brown & Roshko (1974). The streamwise vortices and the mechanisms by which they lead to the generation of small-scale motion are the subjects of the present experimental investigation.

Flow visualization of a chemically reacting liquid shear layer with a visible reaction product (Breidenthal 1981) reveals the evolution of spanwise non-uniformities along the primary (spanwise) vortices. This non-uniformity (dubbed 'wiggle') may be described as being nominally sinuous with considerable variation in spanwise wavelength. As the sinuous structure is convected downstream, its amplitude grows rapidly (apparently as a result of stretching by consecutive primary vortices), with no appreciable change in spanwise wavelength. While there is no evidence that the 'wiggle' is associated with a spanwise instability of the primary vortex core, there is no doubt that its appearance marks the formation of streamwise vortical structures. In plan-view time-exposure photographs, these streamwise vortices appear as continuous streaks, starting at approximately the streamwise onset of the wiggle, and having spanwise spacings which correspond to the wiggle's undulations. Farther downstream the streaks are obscured by a marked increase in (visible) reaction product.

Time-exposure photographs were also obtained by Konrad (1976) and Bernal & Roshko (1986) over a large range of Reynolds number (*Re*) in a non-reactive gas mixing-layer facility. These authors found that the mean onset *Re* of the streaks increases with the shear-layer velocity ratio, and although they are not necessarily equally spaced over a considerable distance downstream of the flow partition, their mean spanwise spacing scales with the vorticity thickness at the streamwise location where they first became visible. Similar observations were reported by Miksad (1972). Contour plots of time-averaged streamwise velocity in a plan view at a fixed cross-stream elevation (Jimenez 1983) closely resemble the streamwise streaks in the time-exposure photographs. An important feature common to these observations is the preservation of spatial coherence and spanwise spacings of the streaks, despite concomitant pairing of the primary vortices.

Based on flow visualization and high-speed cinematography, Bernal (1981) and Bernal & Roshko (1986) suggested that the counter-rotating streamwise vortex pairs in the plane mixing layer are part of a vortex that continuously loops back and forth in the braid region between adjacent spanwise vortices. The mean spanwise spacing of the streamwise vortices appears to increase somewhat as they are convected downstream, although at a much smaller rate than the rate of change in the cross-stream (or streamwise) dimension of the primary vortices. A somewhat different view concerning the structure of the streamwise vortices was proposed by Hussain (1983). Unlike the model of Bernal and Roshko, Hussain's model emphasizes that the braid region is comprised of slender discrete vortices (dubbed 'ribs') randomly displaced with respect to each other in directions normal to their axes.

A number of numerical and analytical studies have shown that the streamwise vortical structures can result from non-uniformities of the spanwise vorticity in the braid region between the primary vortices. Lin & Corcos (1984) showed that a weak spanwise-periodic variation of streamwise vorticity in a uniform straining flow (as between two consecutive spanwise vortices) can evolve into concentrated round streamwise vortices. These findings were further confirmed by Ashurst & Meiburg (1988) via simulations based on inviscid vortex dynamics. The direct Navier–Stokes simulations of Metcalfe *et al.* (1987) show that spanwise instability modes triggered by upstream non-uniformities in the spanwise vorticity are convected with the flow, grow at rates similar to those of the two-dimensional modes, and lead to the formation of pairs of counter-rotating streamwise vortices in the braid region. Metcalfe *et al.* also remark that pairing of the primary vortices may inhibit the three-dimensional instability, while suppression of pairing may drive the three-dimensional modes to turbulent-like states.

Experimental evidence suggests that the streamwise vortices tend to lock onto small geometric details (imperfections in the flow partition, orientation of screens, etc.) in the experimental apparatus (Bernal 1981; Jimenez 1983). Lasheras, Cho & Maxworthy (1986) showed that small vortex-generating elements mounted on the flow partition could move the origin of these vortices considerably upstream; in the absence of these devices and by careful removal of flow disturbances, the origin could be displaced significantly downstream. In related flow visualization experiments, Lasheras & Choi (1988) studied the evolution of a spanwise-periodic pattern of streamwise vortices produced by flow partitions with corrugated and indented trailing edges. Recent experiments in a plane mixing layer excited by a spanwise array of surface film heaters (Nygaard 1987; Fiedler, Glezer & Wygnanski 1988) conclusively demonstrate the ease with which a nearly arbitrary spanwise distribution of streamwise vortices can be generated.

An important feature of the time-exposure photographs of Bernal & Roshko (1986) is the gradual disappearance of the streamwise streaks downstream of where they exhibit remarkable spanwise coherence. Spanwise plots of time-averaged streamwise velocity at a number of streamwise stations (Huang & Ho 1990) show a slow streamwise increase of a characteristic spanwise spacing, indicating either loss of spanwise coherence or disappearance of streamwise structures. Bernal & Roshko further reported that in the region where time-exposure photographs no longer show the presence of streaks, single snapshots show streamwise vortices having mean spanwise spacing nominally larger than that of the upstream streaks. Furthermore, the spanwise locations of these streamwise vortices vary with downstream distance in a manner clearly unrelated to (fixed) structural features of the experimental apparatus.

It is clear that time-invariant spanwise vorticity non-uniformities due to irregularities of the experimental apparatus upstream of the trailing edge of the flow partition, continuously influence the vortex sheet which subsequently becomes part of the spanwise vortices and the braid region. Although spanwise vorticity non-uniformities within the braid region lead to the formation of streamwise vortices, experimental and numerical evidence suggests that under some conditions the same disturbances cause little or no distortion of the primary vortices. In the vortex simulations of Ashurst & Meiburg (1988), an initial spanwise-periodic perturbation leads to the formation of streamwise vortices in the braid region but has little effect on the primary vortices themselves. An out-of-phase waviness of the cores of the primary vortices, observed in the early stages of the numerical simulations of Ashurst and Meiburg, is also observed downstream in the experiments of Lasheras & Choi (1988). In both of these investigations, the waviness of the primary vortices seems to decay downstream due to the continuous rotation of their cores. We further note that in the experiments of Lasheras & Choi streamwise-continuous vortex pairs appear immediately downstream of a flow partition with an indented trailing edge, considerably upstream of the first rollup of the primary vortices. These findings suggest that formation of streamwise vortices in close proximity to the flow partition is mainly the result of upstream non-uniformities in either the experimental apparatus or the flow partition's boundary layers. On the other hand, the observations of Bernal & Roshko (1986) regarding the appearance of streamwise vortices uninfluenced by upstream conditions indicate that, far enough downstream of the flow partition, streamwise vortices may result from an instability of the primary vortices. A spanwise core instability of the primary vortices is a viable mechanism because it is accompanied by distortion of the strain field in the braid region.

Pierrehumbert & Widnall (1982) identified two spanwise instability modes of the primary vortices in their analysis of a shear layer modelled by an array of Stuart vortices. The first mode, referred to as 'translative instability', is spanwise and streamwise periodic. The streamwise wavelength is that of the two-dimensional flow. The most unstable translative disturbance has a spanwise wavelength equal to two-

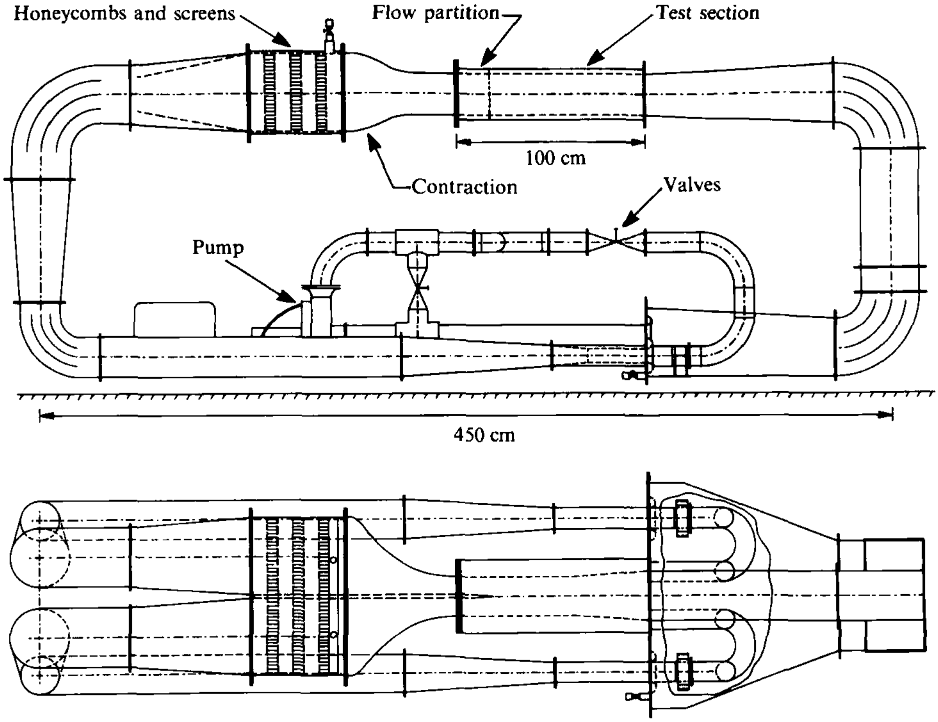

FIGURE 1. Water shear-layer facility.

thirds the spacing of the undisturbed vortices, although disturbances amplify within a broad band of wavelengths. The authors suggest that the translative instability leads to the formation of streamwise vortices observed in the experiments of Breidenthal (1981). Corcos & Lin (1984) assert that rollup of spanwise vorticity into a streamwise-periodic array of vortices gives rise to a translative core instability which allows spanwise perturbations to grow in such a way that the spanwise vortices are identically distorted. Pierrehumbert (1986) later showed that elliptic two-dimensional vortices are unstable to three-dimensional perturbations with spanwise wavelengths much smaller than the characteristic vortex core dimensions. Pierrehumbert proposed this short-wave instability as a mechanism for the direct transfer of energy from the spanwise vortices into fine-scale turbulence. The second instability mode discussed by Pierrehumbert & Widnall (1982) corresponds to spanwise-localized pairing of the primary vortices. This instability mode has a streamwise wavelength twice that of the two-dimensional base flow and, in contrast to the translative instability, has a short spanwise-wavelength cutoff. Experimental evidence that the primary vortices are subject to a core instability having a spanwise wavelength longer than the streamwise (Kelvin–Helmholtz) wavelength is also found in the work of Chandrsuda *et al.* (1978) and Browand & Troutt (1980, 1985). Some aspects of the core instability have been studied recently by Nygaard & Glezer (1990, 1991).

The present work focuses on the evolution of streamwise vortical structures resulting from spanwise-periodic time-harmonic disturbances upstream of the trailing edge of the flow partition. Although the findings of Breidenthal (1981) and Bernal & Roshko (1986) indicate that these streamwise vortices play a crucial role in the mixing transition of the plane shear layer, the mechanism by which small-scale motions necessary for such transition are generated has not been studied. The present investigation is also concerned with open questions regarding details of the formation process of the streamwise vortices, their spanwise spacings, their effect on the two-dimensional base flow, and their interaction with the spanwise vortices.

Section 2 describes the closed-return water shear-layer facility in which the research is conducted, along with the experimental techniques employed. In §3 we discuss the formation of streamwise vortices downstream of the flow partition, their structure, and their role in the mixing transition. Concluding remarks are presented in §4.

2. Facility, actuators, and flow visualization

2.1. *The water shear-layer facility*

The facility is shown in figure 1. The entire flow is driven by a single pump powered by a 10-h.p. motor equipped with a solid-state speed controller. The velocity of each stream can be independently varied, and test-section velocities up to 200 cm/s can be realized. Two interchangeable 100 cm long test sections with cross-sections of 10×22 cm and 22×22 cm are equipped with Lucite walls so that the flow can be observed from any direction. The convergence of the test section on either side of the shear layer can be adjusted easily in order to vary the streamwise pressure gradient. Two interchangeable contractions (with contraction ratios of 7:1 and 9:1) have rectangular cross-sections with constant aspect ratios. Turning vanes and 'turbulence manipulators' (honeycomb and screens) upstream of the contraction reduce velocity variations due to secondary flow. The turbulence level in the free streams is less than 0.15%. The replaceable trailing edges of the flow partition are configured with various mosaics of surface heaters for flow manipulation, described in §2.2.

The facility is equipped with a suite of diagnostic instrumentation. A pressure transducer is connected to two 12-port fast switches. These switches are computer controlled and allow monitoring of the velocity on either side of the contraction exit plane and the static pressure along the test section, as well as Pitot-static measurements of the velocity field within the test section. The water temperature is monitored and recorded by the laboratory computer via a digital thermometer. Fifteen dye injection ports are available on each side of the flow partition. A computer-controlled two-axis traverse mechanism, designed for detailed measurements of the flow field within the test section with rakes of hot-wire probes, has been installed. Twenty channels of hot-wire/film anemometry (AA Labs) are available for simultaneous measurement of instantaneous velocity distributions. A rake of 31 hot-wire sensors, 2 mm apart and suitable for use in water, is mounted on the traverse mechanism for simultaneous cross-stream or spanwise measurement of the streamwise velocity. A Masscomp laboratory computer system, including 16 channels of 12 bit A/D, 16 channels of D/A, and 32 channels of general-purpose I/O, is dedicated to experiment control and data processing.

2.2. *Excitation by surface film heaters*

Excitation of streamwise and spanwise instability modes is accomplished by either of two mosaics of surface film heating elements mounted on the flow partition. Mosaic I consists of 14 spanwise-uniform elements and two 16-element spanwise rows. Mosaic II is comprised of four spanwise-uniform elements upstream of a single

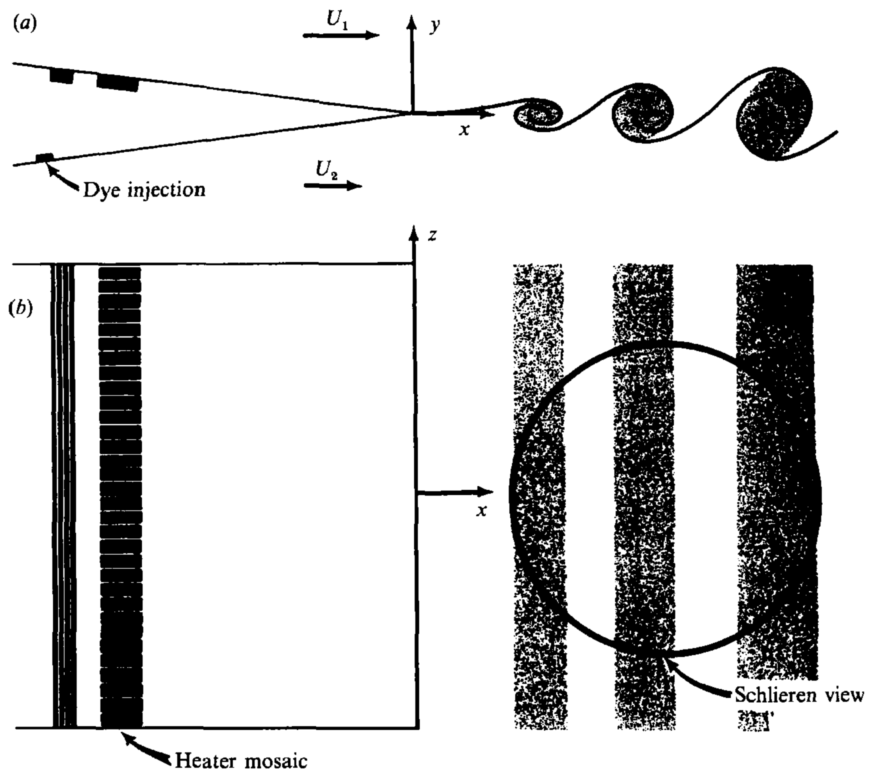

FIGURE 2. Schematic drawings of (a) cross-stream and (b) span views of flow partition. The span view shows heating Mosaic II, which is comprised of four spanwise-continuous elements upstream of a linear array of 32 elements. Also shown is the Schlieren view.

32-element spanwise row. Figure 2 is a schematic drawing of Mosaic II, the flow partition, and the coordinate system. (In the present work x, y, and z are the streamwise, cross-stream, and spanwise coordinates, respectively; the corresponding velocity components are u, v, and w.) The heating elements are mounted on a standard epoxy board substrate. A thin film coating provides good heat conduction, corrosion protection, and electrical insulation. Each heating element is wired through the epoxy board (using through-hole plating) and the flow partition to a DC power amplifier. Thirty-two channels of power amplifiers, each capable of continuously driving 10 A into a load of 2–4 Ω, are available. The unit's output is limited to 2.5 kW by the power supply. Sixteen channels of power amplifiers can be directly driven by the laboratory computer via a D/A interface. This allows input of arbitrary temporal waveforms to the heaters without distortion, by compensating in software for the temperature dependence of the heater resistance and for the quadratic dependence of Joulean dissipation on input voltage. The input power to the heaters is given by $E_0(z)+E(z,t)$, where $E_0(z)$ is the mean power.

The effect of heating the surface is essentially to introduce three-dimensional vorticity perturbations into the flow-partition boundary layer by exploiting the dependence of the viscosity on temperature (Liepmann, Brown & Nosenchuck 1982). It is important to recognize that small oscillations induced in the boundary layer amplify or decay according to linear stability theory. Thus, forcing a shear layer from an upstream boundary layer may not be effective if the induced waves decay

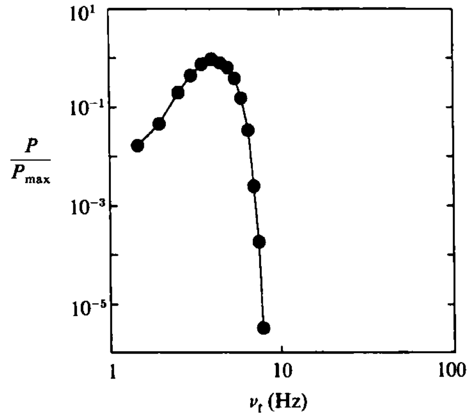

FIGURE 3. Power spectra $P(\nu_f)$ of the streamwise velocity component in response to spanwise-uniform harmonic excitation, where ν_f is the excitation frequency and $P(\nu_f)$ is measured at 2.5 cm downstream of the flow partition and 1 cm above its centreline.

appreciably before reaching the trailing edge. Hence the forcing frequency should be within the unstable (amplified) range of the boundary layer, the extent of which depends strongly on the pressure gradient. By carefully extending the flow partition into the test section, the streamwise pressure gradient can be tuned so that it becomes slightly adverse, causing the flow-partition boundary layer to become less stable and more receptive to forcing.

The response of the flow to spanwise-uniform harmonic excitation over a range of forcing frequencies is deduced from power spectra $P(\nu)$ of the streamwise velocity 2.5 cm downstream of the flow partition and 1 cm above its centreline (on the high-speed side). The free-stream velocities are $U_1 = 30$ cm/s, and $U_2 = 10$ cm/s. These free-stream velocities are used in all the present experiments with the exception of the experiments described in §3.1. Several runs over a range of forcing frequencies ν_f were made. Figure 3 shows $P(\nu_f)$ as a function of ν_f, indicating the composite receptivity of the high-speed-side boundary layer and the shear layer to spanwise-uniform harmonic excitation. In connection with these measurements it is important to note that the hot-wire probe is operated at a 4% overheat ratio, which renders it sensitive to temperature variations of the order of 0.1 °C. As shown in figure 3, the probe does not respond to heater excitation at frequencies outside of a relatively narrow bandwidth, and hence it may be concluded that shear-layer temperature fluctuations associated with the surface heating are very small. Furthermore, the importance of buoyancy effects in forced-convection boundary layers may be evaluated (Schlichting 1968) based on the ratio $\gamma = Gr/(Re_{\delta*})^2$ where Gr is the local Grashof number. For the largest surface overheat we compute $\gamma < 10^{-3}$. Buoyancy effects can be neglected if $\gamma \ll 1$.

Figure 4 shows cross-stream profiles of the dimensionless streamwise velocity $\hat{U}(\eta) = [U(\eta) - U_2]/\Delta U$, plotted as a function of the usual similarity variable $\eta = (y-y_0)/(x-x_0)$, where $U(\eta)$ is the mean velocity measured at a number of streamwise stations, x_0 is the virtual origin, and $\Delta U = U_1 - U_2$. Here, $y_0(x)$ is the cross-stream elevation at which $U(x,y) = \frac{1}{2}(U_1+U_2)$, hereinafter defined as U_c. The flow is excited near the 'natural' frequency and its first subharmonic (6 and 3 Hz, respectively) using spanwise-uniform excitation from Mosaic I (corresponding velocity profiles using Mosaic II are shown in figure 12 below). These data demonstrate that in the

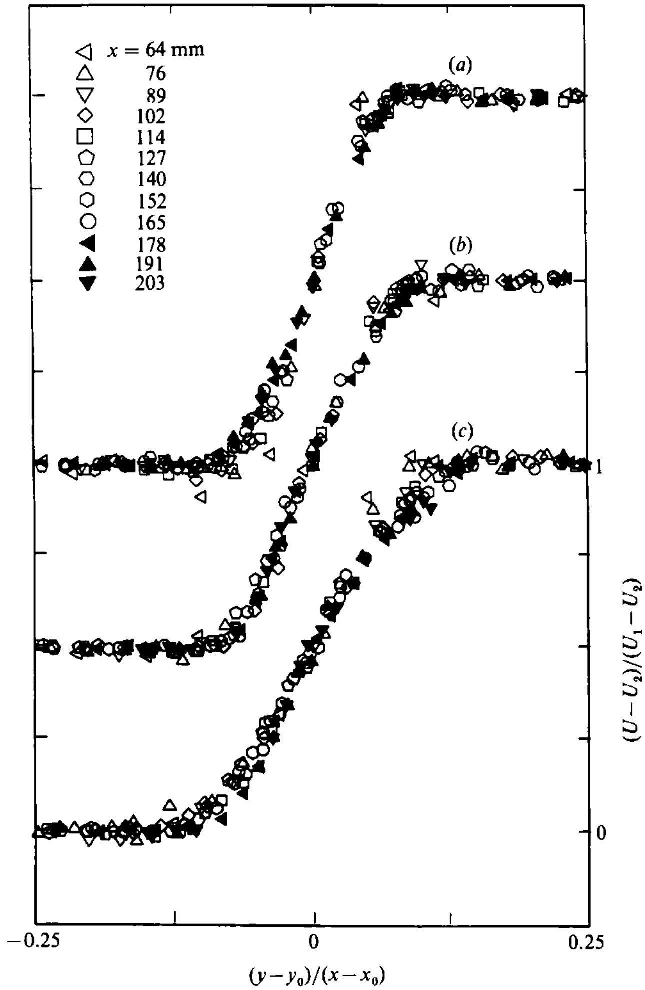

FIGURE 4. Mean streamwise velocity profiles at 12 equally spaced streamwise stations (6.4 cm $\leqslant x \leqslant$ 20.3 cm). Unforced (*a*), and with spanwise-uniform harmonic excitation: ν_f = 6 Hz (*b*), and ν_f = 3 Hz (*c*).

streamwise domain considered here the forced shear layer spreads more in the cross-stream direction than does the unforced flow, in agreement with the findings of other investigators (e.g. Oster & Wygnanski 1982).

In figure 5(*a*–*c*) we show power spectra $P(\nu)$ of the streamwise velocity at x = 10.2 cm ($Re_\theta = 216$), 17.8 cm ($Re_\theta = 663$), and 25.4 cm ($Re_\theta = 1450$) for $y = y_0$. The Reynolds numbers at these x-stations are based on the momentum thickness

$$\theta(x) = \frac{1}{(\Delta U)^2}\int_{-\infty}^{\infty} [U(x)-U_2][U_1-U(x)]\,\mathrm{d}y.$$

The spectra in figure 5(*b*, *c*) correspond to spanwise-uniform harmonic excitation at ν_f = 6 and 3 Hz, respectively. The establishment of small-scale motion in free shear flows is often connected with the existence of an inertial subrange in which the slope of log $P(\nu)$ versus log ν is $-\frac{5}{3}$. At sufficiently high Reynolds numbers in a homogeneous, stationary, and isotropic turbulent flow, the inertial subrange is the

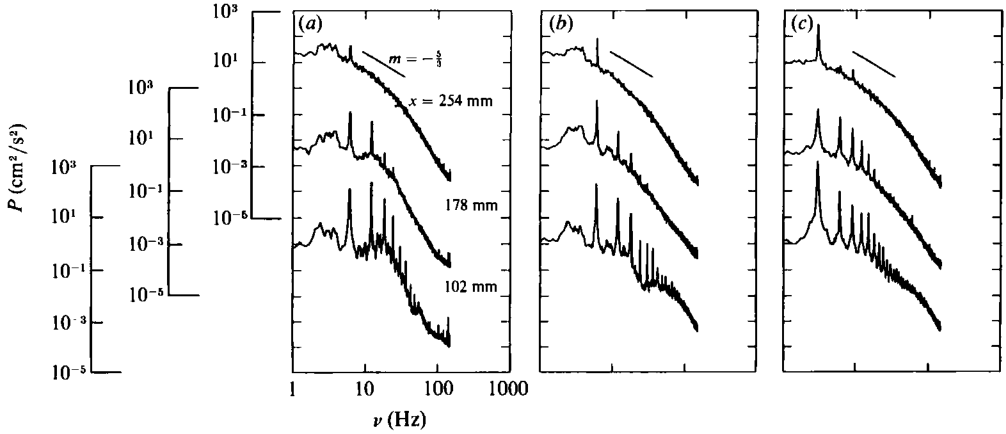

FIGURE 5. Evolution of $P(\nu)$ with x ($x = 10.2$, 17.8, 25.4 cm). Unforced (a), and with spanwise-uniform harmonic excitation: $\nu_f = 6$ Hz (b), and $\nu_f = 3$ Hz (c). Data are measured at $y = y_0$.

low-wavenumber part of an equilibrium range of wavenumbers in which negligible viscous dissipation occurs (Batchelor 1953). Free shear flows, however, are not homogeneous, and if forced, are not statistically stationary, so that the extent of the inertial subrange (which implies local isotropy) in laboratory flows is limited even at relatively high Reynolds number (Champagne 1978). Furthermore, mixing transition does not depend on the existence of an inertial subrange, but rather on the presence of turbulence or fine-scale random vortical structures, which can exist even at relatively low Reynolds numbers. In fact, the characteristic time necessary for establishment of an inertial subrange may lead to its appearance farther downstream from where mixing transition takes place. In the present experiments the inertial subrange at $x = 25.4$ cm is estimated to be 5 Hz $< \nu <$ 32 Hz (cf. Jimenez, Martinez-Val & Rebollo 1979), and the logarithmic slope of the power spectrum within this subrange is approximately $-\frac{5}{3}$. Ho & Huerre (1984) assert that typical transition Reynolds numbers in liquids fall in the range $750 < Re_\theta < 1700$.

2.3. *Flow visualization*

Introduction of a controlled vorticity distribution into the boundary layer of the flow partition by the surface heaters is accompanied by small localized density gradients in the adjacent fluid. The corresponding refractive index gradients are exploited for flow visualization by means of a sensitive double-pass Schlieren system (Fiedler *et al.* 1985). This technique allows the effect of forcing to be studied non-intrusively in planes parallel and normal to the flow span. The Schlieren view can be thought of as a planar projection of streaklines of slightly heated fluid elements. In the present investigation the Schlieren view is in the spanwise (x, y)-plane of the mixing layer and consists of a 13.2 cm diameter circle centred in midspan. Because the flow is forced, two Schlieren views photographed at the same phase relative to the excitation waveform and centred 7.6 cm and 15.2 cm downstream of the trailing edge of the flow partition can be combined into a composite showing the flow for 1 cm $\leqslant x \leqslant$ 21.8 cm.

Photographs of the flow subjected to spanwise-uniform 5 Hz harmonic excitation are shown in figure 6(a, b). The flow is from left to right. In the cross-stream (x, y)-plane (figure 6a) the flow is visualized by dye injected into the boundary layer of the low-speed side at midspan. In the spanwise (x, z)-plane, visualization was accomplished by the Schlieren technique described above. The two views have the

(a)

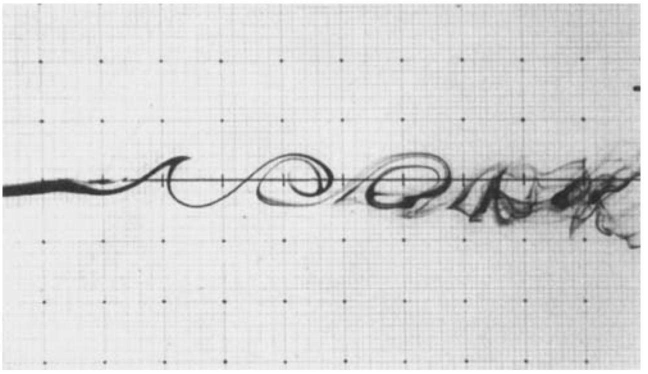

(b)

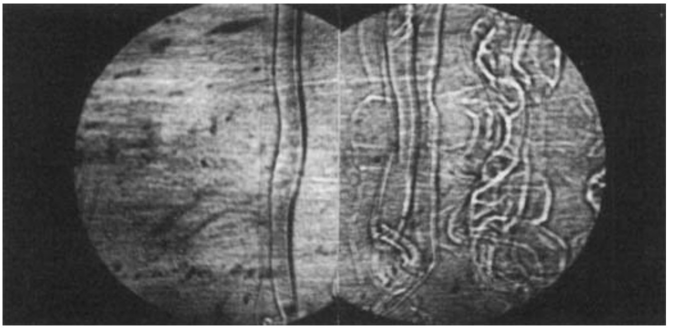

FIGURE 6. (a) Side (x, y) and (b) plan (x, z) views showing the streamwise evolution of spanwise-uniform harmonic excitation ($U_1 = 30$ cm/s, $U_2 = 10$ cm/s, $\nu_t = 5$ Hz). The side and plan views are dye (injected at midspan) and Schlieren visualizations, respectively. They have the same scale and are photographed at the same phase relative to the excitation waveform. The grid in (a) is square and measures 2.54 cm on the side. The plan view in (b) is 20.2 cm long and 13.2 cm wide (in the x- and z-directions, respectively). Its upstream edge begins at $x = 1$ cm.

same scale, begin (at the left-hand side) 1 cm downstream of the flow partition, and were separately photographed at the same phase relative to the zero crossings of the excitation signal. At this excitation frequency, pairing of the primary vortices does not occur in the streamwise domain shown here.

Although streaklines of coloured or heated fluid elements do not necessarily mark the presence of vorticity, they strongly suggest the formation of spanwise-coherent vortices. It is important to recognize that the Schlieren view is a planar projection in the cross-stream direction (i.e. a y-integration) from which depth information has been lost. The Schlieren image of the primary vortex immediately downstream of the first rollup (figure 6b) is characterized by sharp intensity gradients along its upstream and downstream edges caused by the strong curvature of the thin layer of heated fluid which is rolled into the vortex. The slight spanwise non-uniformity in the instantaneous visualization shown in figure 6(b) also characterizes the ensemble-averaged flow (cf. figure 10(a) and the accompanying discussion in §3.3). Since the excitation waveform corresponding to figure 6(b) is spanwise uniform, these results also suggest the formation of naturally occurring streamwise vortices in the braid region, as well as the evolution of spanwise non-uniformities in the cores of the primary vortices. The development of small-scale motion within the cores of the spanwise vortices is apparent at the downstream end of the composite Schlieren view.

As noted by M. Landahl (private communication 1990), streamwise streaks in transitional flat-plate boundary layers have been identified as regions of high- or low-speed velocity perturbations not necessarily associated with continuous concentrations of streamwise vorticity. Nevertheless, because of the remarkable similarity between the present flow visualization and three-dimensional cross-stream and streamwise vorticity concentrations in the numerical simulations of Rogers & Moser (1989) and Buell & Mansour (1989), we hereinafter refer to streamwise streaks in our Schlieren flow visualization as streamwise vortices. We emphasize that reference to a 'streamwise vortex' in the present work does not refer to a domain containing only streamwise vorticity, nor does it imply that the axis of the vortex is parallel to the streamwise direction.

3. Structure and evolution of streamwise vortices

Several experimental investigations of plane mixing layers have demonstrated that streamwise vortices in the braid region can be triggered by spanwise-non-uniform excitation using either passive (e.g. Lasheras & Choi 1988; Bell & Mehta 1989) or active (Nygaard & Glezer 1989) devices mounted on the flow partition. Because evolution of the streamwise vortical structures appears to be phase-locked to the two-dimensional instability of the base flow, an important attribute of active devices such as our surface heaters is that they allow for streamwise and spanwise instability modes to be excited relatively independently. Spanwise-uniform time-harmonic excitation provides a powerful tool for the manipulation of some streamwise instability modes, with dramatic global effects on the flow. In particular, forcing at the natural (most unstable) frequency produces a region downstream of the flow partition in which the passage frequency of the primary vortices is equal to the forcing frequency and pairing is inhibited (e.g. Roberts 1985). Thus, the evolution of the streamwise vortices can be studied phase-locked to the excitation waveform and in the absence of interactions between the primary vortices.

In a previous investigation (Nygaard 1987; Fiedler *et al.* 1988) we studied the effect of spanwise-non-uniform harmonic excitation

$$E(z,t) = A(z)\sin(\omega_f t)$$

on the evolution of the streamwise vortices at relatively low free-stream velocities (18 and 6 cm/s). The streamwise vortices form at spanwise locations corresponding to minima of $A(z)$ and, at least close to the flow partition, resemble lambda vortices in transitional flat-plate boundary layers (e.g. Saric & Thomas 1983). Within the spanwise resolution of the heating mosaic, the shape of the streamwise vortices was almost invariant with respect to different spanwise-periodic waveforms $A(z)$ having the same spanwise wavelength λ_z.

In this section we discuss two experiments. The first (§3.1) is a study of the early stages in the formation of the streamwise vortices. The second (§§3.2–3.5) is a study of the interaction between the streamwise and spanwise vortices and the subsequent generation of small-scale motion necessary for mixing transition. In both experiments pairing of the spanwise vortices is inhibited by choosing ν_f to be approximately equal to the natural frequency of the mixing layer. Measurements of the streamwise velocity component are obtained using the hot-wire rake described in §2.1. The

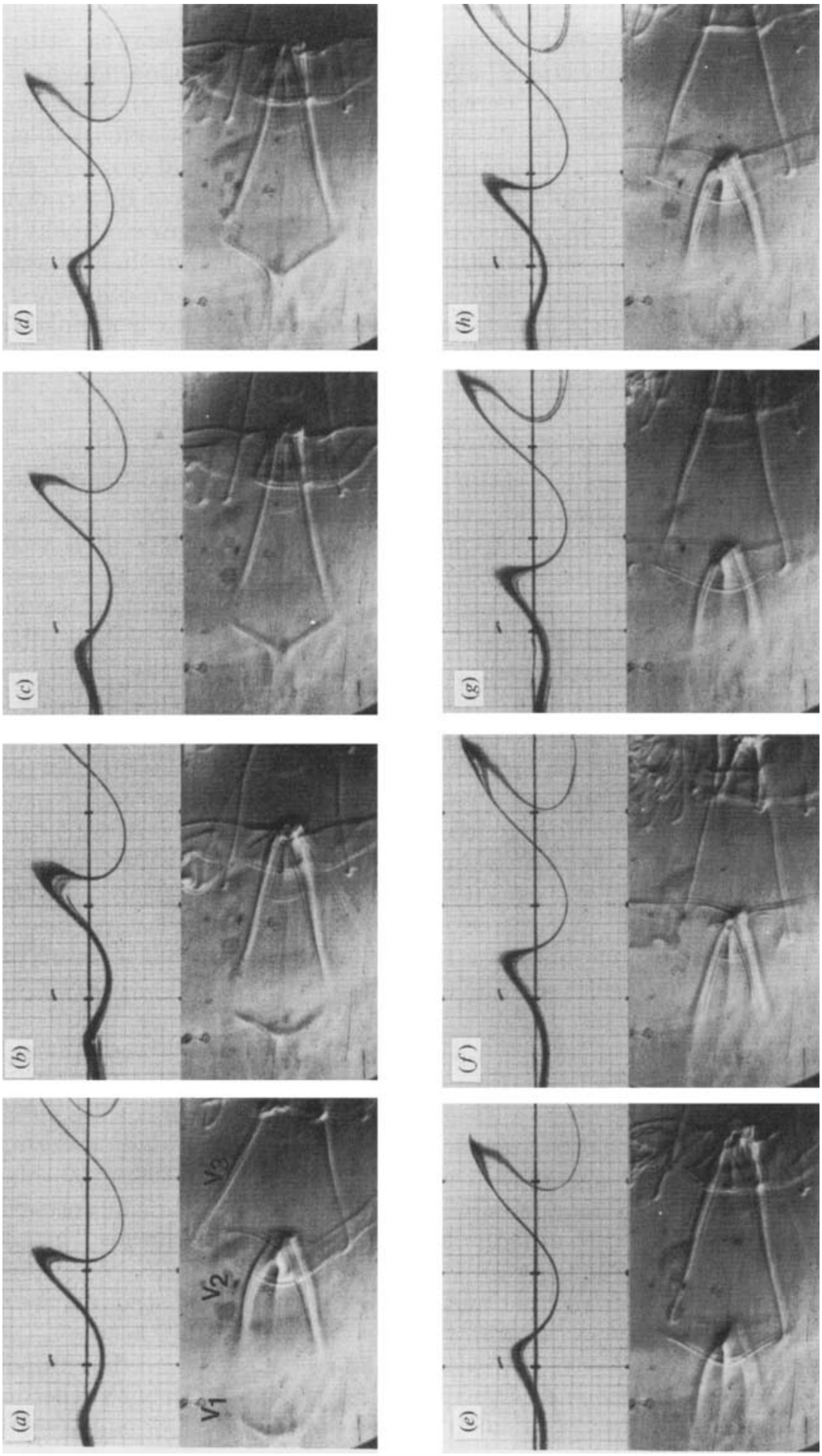

FIGURE 7. Composite of eight pairs of side and plan views photographed at equal time intervals during the excitation period and showing the streamwise evolution of a spanwise-isolated streamwise vortex ($U_1 = 25$ cm/s, $U_2 = 9$ cm/s). The two views of each pair are photographed at the same phase relative to the excitation wavetrain. Heating Mosaic I is used to synthesize a 16-element discretization of $1 - \cos(2\pi z/\lambda_z)$, where $\lambda_z = 6.35$ cm and the frequency of the harmonic wavetrain is $\nu_t = 3.7$ Hz. The field of view is 9.65 cm long (in the x-direction) and begins at $x = 2.54$ cm.

length of the velocity time series at each measurement point corresponds to 400 cycles of the harmonic excitation. The data are sampled at $128\nu_f$.

3.1. *Formation of the streamwise vortices*

The evolution of a spanwise-isolated streamwise vortex was studied by using heating Mosaic I to synthesize a steady 16-element discretization of $E_0(z) = 1-\cos(2\pi z/\lambda_z)$, where λ_z is equal to the width of 10 heating elements. Because phase jitter in the passage frequency of the spanwise vortices at the measurement station decreases with U_c, the velocities of the two streams are reduced to 25 and 9 cm/s and the corresponding excitation frequency is $\nu_f = 3.7$ Hz. During excitation of the spanwise-uniform wavetrain, the flow is illuminated in the (x, z)-plane by a strobe triggered at a phase delay relative to the zero crossings of $E(z, t)$, and photographed using the Schlieren technique described in §2.3. The flow in the (y, z)-plane was visualized by means of dye injection in the low-speed side and was photographed separately at the same phase relative to the zero crossings of $E(z, t)$. Figure 7(*a–h*) is a composite of eight pairs of side (x, y)- and span (x, z)-views taken at equal time intervals during the excitation period. The field of view is between 2.5 and 12.4 cm downstream of the flow partition.

Figure 7(*a–c*) suggests that spanwise-non-uniform vorticity concentrations (at the upstream (left) end of the (x, z)-view in figure 7*a*), referred to below as V_1, first appear on the crest of the two-dimensional wave, *prior* to rollup of the vortex sheet into a primary vortex. (As noted in §2.3, the Schlieren visualization of the rollup of the spanwise vortex is characterized by sharp intensity gradients along its upstream and downstream edges.) Owing to the spanwise-non-uniform excitation, V_1 develops an upstream bend about its middle as it is advected downstream. The streamwise vortices formed during previous cycles of the excitation wavetrain are observed at the centre and downstream end of the Schlieren view in figure 7(*a*) (referred to below as V_2 and V_3, respectively). In figure 7(*b–d*) the legs of V_2 appear to be connected to V_1 and form a nearly quadrilateral vortex structure embedded in the deformed vortex sheet, marked by dye in the corresponding side view. The downstream edge of the quadrilateral structure lies on the high-speed side of a spanwise vortex, while the upstream edge is deformed and stretched by rollup of the following spanwise vortex.

As a result of stretching of V_1 and rollup of the spanwise vortex sheet, a new hairpin eddy-like structure forms near the region of maximum curvature of the upstream bend (figure 7*e*). Previous experimental work on the formation of streamwise vortices in the braid region (Lasheras *et al.* 1986; Lasheras & Choi 1988) emphasizes that streamwise vortices begin to form near a stagnation point (in a reference frame moving with U_c) between two adjacent spanwise vortices and are subsequently stretched continuously in the upstream and downstream directions. Figure 7(*a–h*) suggests that variations in the streamwise strain field due to the Kelvin–Helmholtz instability lead to formation of streamwise vortices even before rollup of the primary vortices is completed. Streamwise vortices appear near the high-speed edge of a primary vortex during its rollup, and are then continuously stretched in the upstream direction towards the low-velocity side of a subsequent spanwise vortex. Consistent with the numerical simulations of Buell & Mansour (1989), we note that, at least within the streamwise domain shown here, neither the heads nor legs of the hairpin eddies appear to be ingested into the spanwise vortices.

The streamwise location at which streamwise vortices first appear is probably related to the amplitude of the upstream disturbances leading to their formation. In the experiments of Lasheras & Choi (1988) streamwise counter-rotating vortex pairs appear immediately downstream of a flow partition with an indented trailing edge. Huang & Ho (1990) measured substantial levels of narrow-band energy contents of the spanwise velocity component at $Rx/\lambda < 1$ (i.e. before the first rollup of the primary vortices) in an unforced plane mixing layer at relatively high Reynolds number. The authors concluded that streamwise vortices develop together with the primary vortices immediately downstream of the flow partition. While the Lin–Corcos mechanism for the formation of streamwise vortices (Lin & Corcos 1984) may be valid upstream of rollup of the primary vortices, we note that streamwise vorticity can also develop in a spanwise- and streamwise-uniform base flow. An example is the formation of Langmuir circulations in the surface layers of natural waters (Leibovich 1983). These counter-rotating vortex pairs form when wind blows over water, with their axes nearly parallel to the wind and their crosswind (i.e. spanwise) spacing scaling with the vorticity thickness.

While there is no question that spanwise-non-uniform excitation alters the nominally two-dimensional base flow, it is a non-trivial matter to extract a three-dimensional vortical structure from data of a single velocity component. Nevertheless, such a three-dimensional structure would be invaluable as a first step in understanding the dynamics of the flow. Such a vortical structure could be distinguished from the rest of the flow by the high intensity of the r.m.s. velocity fluctuations $u'(\boldsymbol{x},t)$. A scheme by which $u'(\boldsymbol{x},t)$ is computed relative to each individual data record and then ensemble-averaged, $\langle u'_t(\boldsymbol{x},t)\rangle$, has been implemented (Glezer, Katz & Wygnanski 1989). Unlike the conventional $\langle u'\rangle$, the ensemble-average ('true') r.m.s. velocity fluctuations $\langle u'_t\rangle$ are not prone to spurious contributions from low-frequency variations of the flow relative to its mean (e.g. velocity fluctuations outside of the mixing layer induced by passage of spanwise vortices).

The 'true' r.m.s. velocity fluctuations, phase-averaged over the excitation period, are computed from detailed measurements of the streamwise velocity in (y,z)-planes. The data shown in figure 8(a, b) are measured at $x = 15$ cm (corresponding to $X = Rx/\lambda_{\mathrm{KH}} = 3.12$, $R = \Delta U/U_c$ and λ_{KH} is the wavelength of the Kelvin–Helmholtz instability), where $Re_{\theta(x)}$ for the harmonically excited flow is 570. The domain of measurements is rectangular (6×5.2 cm in the y- and z-directions, respectively), and the measurement points are equally spaced (2 mm apart) in each coordinate. The surface $\langle u'_t\rangle = 0.085$ cm/s in (y,z,t)-coordinates is shown during two periods of the spanwise-uniform and spanwise-non-uniform excitation waveforms. Note that in this figure, as in all phase-locked plots below, time increases to the left in order to facilitate comparison with the Schlieren and dye views in which the vortical structures are advected to the right. Although these are not surfaces of constant vorticity, they seem to effectively capture three-dimensional features of the streamwise vortices which are similar to the numerical results of Metcalfe *et al.* (1987) and Buell & Mansour (1989). Our data demonstrate that the streamwise vortex resulting from spanwise-non-uniform excitation induces substantial spanwise variations of $\langle u'_t\rangle$ within the primary vortex and in the braid region. Of particular note is the expansion of turbulent interfaces, probably corresponding to small-scale motion on the high-speed edge of the primary vortex (figure 8b). These modifications of the nominally two-dimensional base flow are further discussed in §3.4.

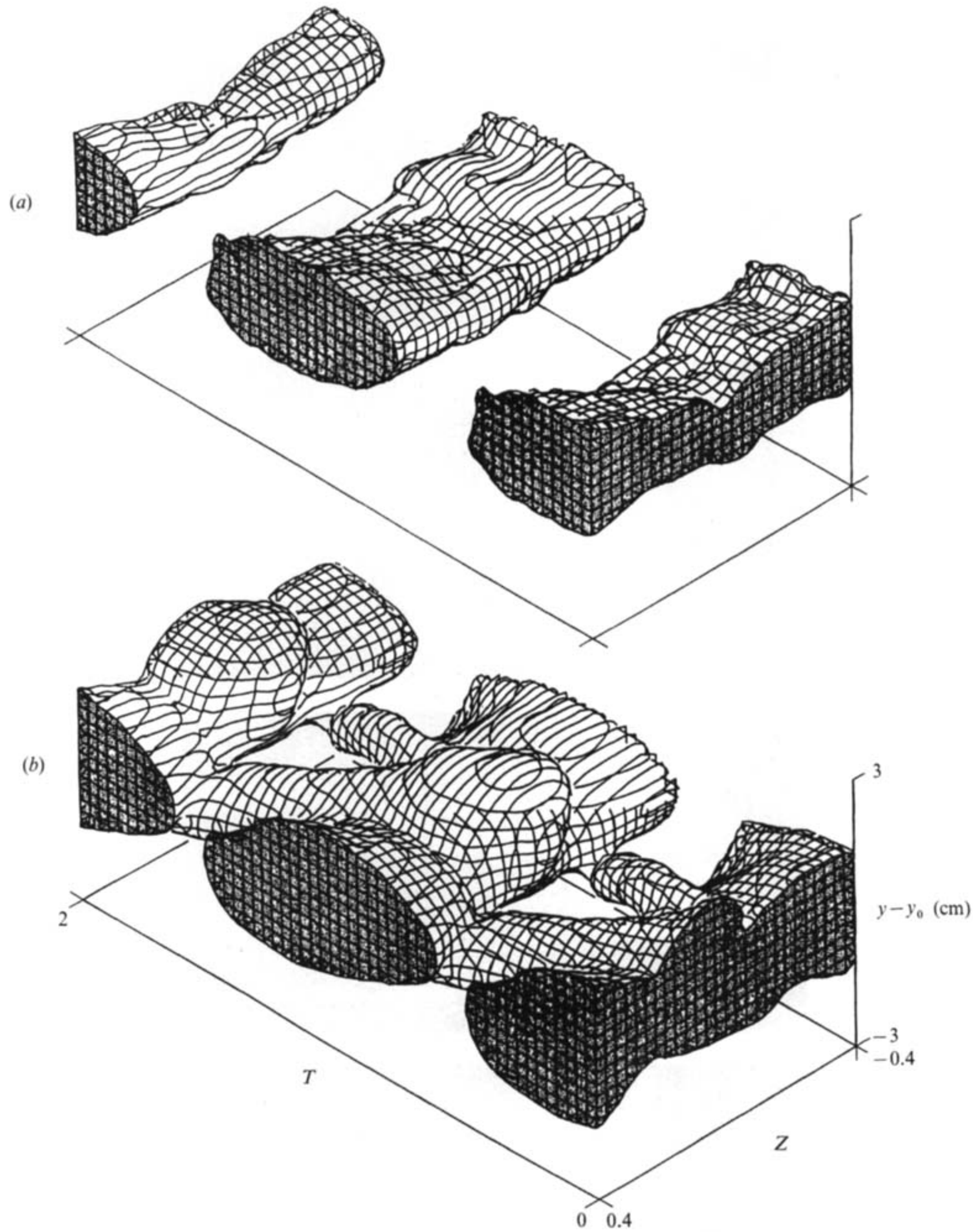

FIGURE 8. The surface $\langle u_t'(y,z,t)\rangle = 0.085$ cm/s, at $x = 15$ cm, during two periods of (*a*) the spanwise-uniform and (*b*) spanwise-non-uniform excitation wavetrains ($Z = z/\lambda_z$, $T = t\nu_t$). Flow conditions as in figure 7.

3.2. *The effect of spanwise wavelength*

In figure 9(*a–d*) we show the effect of λ_z on the ensuing streamwise vortices at higher free-stream velocities (30 and 10 cm/s) and excitation frequency ($\nu_t = 5$ Hz) than discussed in §3.1. The amplitude of the excitation waveform $A(z)$ is piecewise-continuous and spanwise-periodic with wavelength λ_z. To define the waveform, we

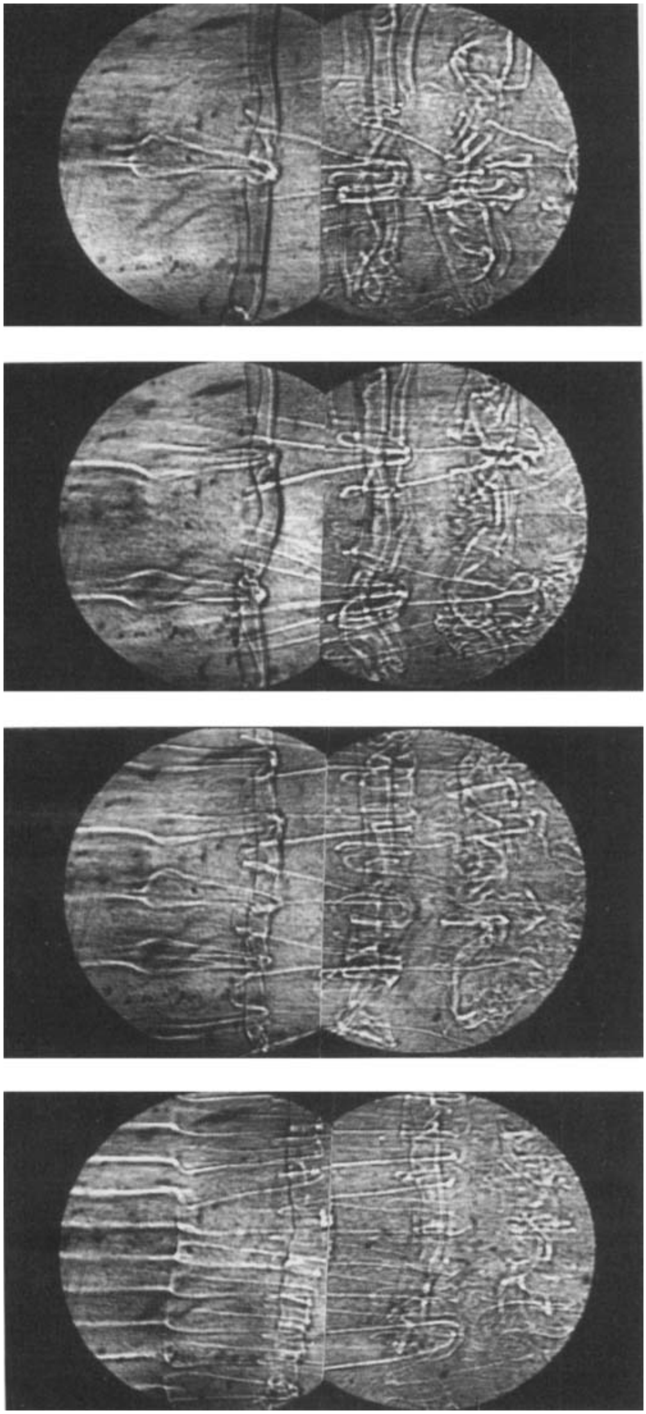

(a)

(b)

(c)

(d)

FIGURE 9. Response of the mixing layer to time-harmonic excitation waveforms having different spanwise wavelengths. (a) $\lambda_z = 10.2$ cm; (b) 5.08 cm; (c) 2.54 cm; (d) 1.27 cm. The field of view and flow conditions are as in figure 6(b).

let $z = z_0 + \lambda_z s$, where z_0 is an arbitrary reference and $0 \leqslant s \leqslant 1$. Then in each wavelength, $A(z)$ is given by $A(z) = A_H$ for $0 \leqslant s \leqslant s_1$, $A(z) = A_L$ for $s_1 \leqslant s \leqslant s_2$, and $A(z) = A_H$ for $s_2 \leqslant s \leqslant 1$. In the present experiments, λ_z is taken as the widths of 2, 4, 8, and 16 elements of Mosaic II (figures 9*a*, 9*b*, 9*c*, 9*d*, respectively), $(s_2 - s_1)\lambda_z$ is equal to the width of one heating element, and $A_L = 0.3A_H$. Because of its deep minima, this waveform is effective in minimizing spanwise jitter in the locations of the ensuing streamwise vortices. All Schlieren views in figure 9(*a–d*) are obtained at the same phase relative to the harmonic wavetrain.

As mentioned above, the forced streamwise vortical structures bear considerable resemblance to lambda vortices in a transitional flat-plate boundary layer. In the present experiments, the included angle Λ between the legs of the streamwise vortices decreases with decreasing λ_z. For relatively long λ_z (e.g. figure 9*b*), Λ is unchanged because spanwise interaction among streamwise vortices is reduced. The existence of spanwise-isolated streamwise vortices for $\lambda_z > \lambda_{KH}$ (figure 9*a*) indicates that these structures are not part of a single vortex that continuously loops back and forth between adjacent spanwise vortices, as conjectured by Bernal & Roshko (1986). Figure 9 further suggests that for a given excitation frequency, virtually any spanwise wavelength synthesizable by the heating mosaic can be excited and can lead to the formation of streamwise vortical structures. This is supported by the flow visualization study of Lasheras & Choi (1988), where the average spanwise spacing of the streamwise vortices (their figure 26*a*) appears to be much smaller than the spanwise wavelength of their corrugated flow partition.

An important aspect of spanwise-non-uniform excitation at long λ_z (typically longer than λ_{KH}) is shown in figure 9(*a*, *b*). In figure 9(*a*) the central spanwise vortex deforms at midspan and develops an upstream bend. As shown in the experiments of Lasheras & Choi (1988), the three-dimensional alignment of the approximately streamwise vortices in the braid region is determined by the orientation of the strain field induced by the primary vortices. The spanwise undulations of the primary vortices modify the strain field in the braid region and consequently induce a significant increase in Λ. Farther downstream, the upstream bend in the spanwise vortex (on the right) is increased, and smaller-scale vortical tubes appear to be formed near the head of the streamwise vortex. When λ_z is reduced (figure 9*b*), the first spanwise vortex downstream of the flow partition (on the left) develops spanwise undulations having the wavelength of the excitation. As in figure 9(*a*), the forced streamwise vortices are located at the upstream bends of these undulations, and Λ increases with downstream distance.

Of particular note are additional vortex tubes which appear along the legs of the streamwise vortex in the braid region between the spanwise vortices in the centre and left of figure 9(*b*). These vortex tubes are probably associated with rollup of the streamwise vortices. Such a mechanism is discussed by Pullin & Jacobs (1986) in their numerical study of the nonlinear evolution of an array of inviscid counter-rotating vortex pairs subjected to an applied stretching strain field. This leads to rollup of multiple 'secondary' streamwise vortices near each of the legs of a 'primary' streamwise vortex. All secondary streamwise vortices associated with a given primary leg have the same sense of rotation. Lasheras *et al.* (1986) studied a streamwise vortex forced by a small hemisphere mounted on the flow partition of a plane mixing layer and proposed an induction mechanism for its spanwise spreading. The appearance of additional vortical tubes in the experiments of Lasheras *et al.* is clearly connected with undulation of the spanwise vortex. This deformation significantly modifies the vorticity and strain distributions in the braid region, and hence may trigger the secondary instability of Pullin & Jacobs. In fact, forced streamwise vortices show little spanwise spreading when the spanwise vorticity remains approximately two-dimensional (figure 9*c*, *d*). An upstream bend of the spanwise vortex is also apparent in the photographs of Lasheras *et al.* (their figure 15, corresponding to figure 9*b* here).

The undulations of the spanwise vortices result from an instability of their cores. Some preliminary results regarding this core instability have been obtained by Nygaard & Glezer (1990). It appears that as a result of this instability, the primary vortices undergo spanwise deformation, the wavelength of which typically exceeds λ_{KH}, and induce secondary vortical structures through deformation of the strain field in the braid region. Although the core instability is apparent in a number of previous experiments (e.g. Chandrsuda *et al.* 1978; Browand & Troutt 1985; and Lasheras & Choi 1988), no previous investigation has established its connection to the formation of streamwise vortices in the braid region.

3.3. *Modification of the two-dimensional base flow by the streamwise vortices*

The response of the flow to spanwise-non-uniform excitation may be evaluated from ensemble-averaged (phase-locked to $E(z,t)$) time series of the streamwise velocity perturbation:

$$\langle u_{\text{pert}}(\boldsymbol{x},t)\rangle = \langle u(\boldsymbol{x},t)\rangle - U(\boldsymbol{x}),$$

where $U(\boldsymbol{x})$ is the mean flow velocity computed from the ensemble-averaged data,

$$U(\boldsymbol{x}) = \frac{1}{t_f}\int_0^{t_f} \langle u(\boldsymbol{x},t)\rangle \,\mathrm{d}t$$

and

$$t_f = 1/\nu_f$$

is the temporal period of $E(z,t)$.

In what follows, we study the effect of spanwise-non-uniform excitation on the nominally two-dimensional base flow. The spanwise wavelength of the excitation waveform $E(z,t)$ is synthesized by four-element groups of Mosaic II ($\lambda_z = 2.54$ cm). An instantaneous Schlieren visualization of the forced flow is shown in figure 9(*c*).

The response of the mixing layer to spanwise-uniform and spanwise-non-uniform excitation close to the trailing edge of the flow partition is shown in figure 10(*a*) and 10(*b*), respectively, using contour plots of $\langle u_{\text{pert}}(z,t)\rangle$ measured at $x = 5.1$ cm ($X = 1.27$), and $y = y_0$. The duration of the ensemble-averaged time series is $4t_f$, and the data are taken equidistantly (2.5 mm apart) along the span. Shaded regions (indicated by dots) correspond to $\langle u_{\text{pert}}(z,t)\rangle < 0$. (Despite some spanwise non-uniformity (see also figure 6*b*), the base flow is reasonably two-dimensional.) Even though the contour plots in figure 10(*a*, *b*) are planar cross-sections of a three-dimensional flow at a fixed cross-stream elevation, they contain useful structural information. The dark spanwise bands in figure 10(*a*) represent times of most rapid velocity increase (or decrease) and can be associated with phase fronts of the (excited) Kelvin–Helmholtz instability. Note that the y-elevation of the probe is such that $\langle u_{\text{pert}}(z,t)\rangle < 0$ during passage of the (high-speed) crest of the two-dimensional instability wave.

At this streamwise station, the primary vortex rollup has just begun (figure 6*a*), and the vortical structure excited by spanwise-non-uniform heating already has an upstream bend about its middle as it is advected downstream (e.g. figure 7*c*). The induced velocity fluctuations $\langle u_{\text{pert}}(z,t)\rangle$ in figure 10(*b*) are consistent with these

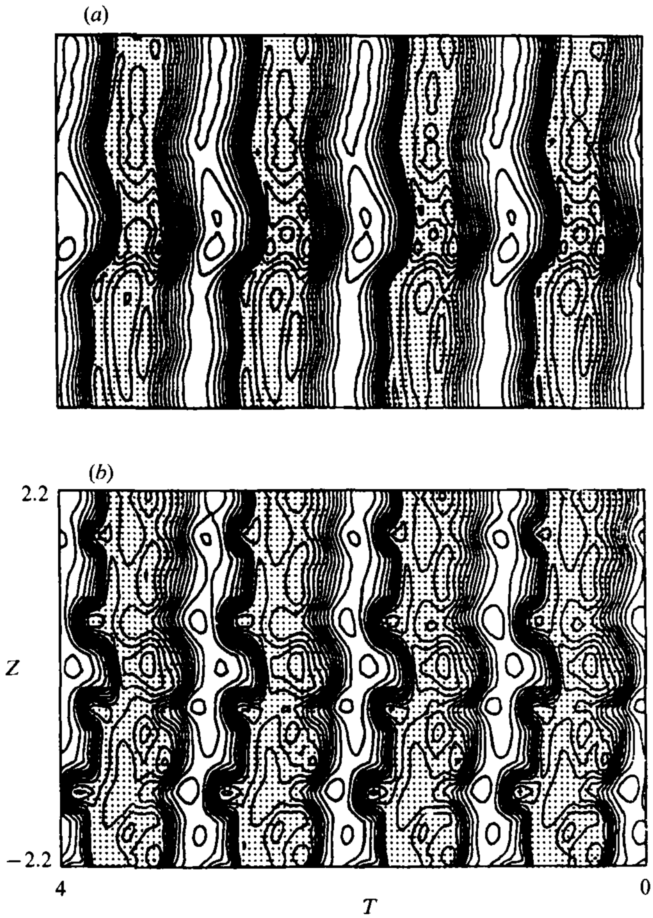

FIGURE 10. Contours of $\langle u_{\text{pert}}(z,t)\rangle$ at $x = 5.1$ cm and $y = y_0$. (*a*) Spanwise-uniform excitation; (*b*) spanwise-non-uniform excitation. Shaded regions correspond to $\langle u_{\text{pert}}(z,t)\rangle < 0$. Contours start at 0, with contour increments of 1.0 (-1.0) cm/s.

observations. As discussed in §3.1, the upstream bend of the streamwise vortical structure first appears on the (high-speed) crest of the two-dimensional wave lying above the cross-stream elevation of the probe at $y = y_0$ (i.e. for $\langle u_{\text{pert}}(z,t)\rangle < 0$ in figure 10*a*). Because the streamwise vortex is advected in a shearing flow, its induced velocity field acts to move fluid down (or up) from higher (or lower) cross-stream elevations. Hence, the streamwise velocity at a given y-elevation may be higher or lower than it would be in the absence of spanwise-non-uniform excitation, and the presence of the streamwise vortices is marked by local minima or maxima of $\langle u_{\text{pert}}(z,t)\rangle$. For example, higher-momentum fluid from the high-speed side is moved down between the counter-rotating legs of a streamwise vortex, and similarly lower-momentum fluid from the low-speed side is moved up between the legs of adjacent streamwise vortices. This results in alternating local maxima and minima of velocity perturbations within the negative (shaded) regions. The strength of velocity perturbations induced by the streamwise vortices is time-periodic because these vortices, inclined in the streamwise direction as they are advected past the measurement station, are themselves time-periodic.

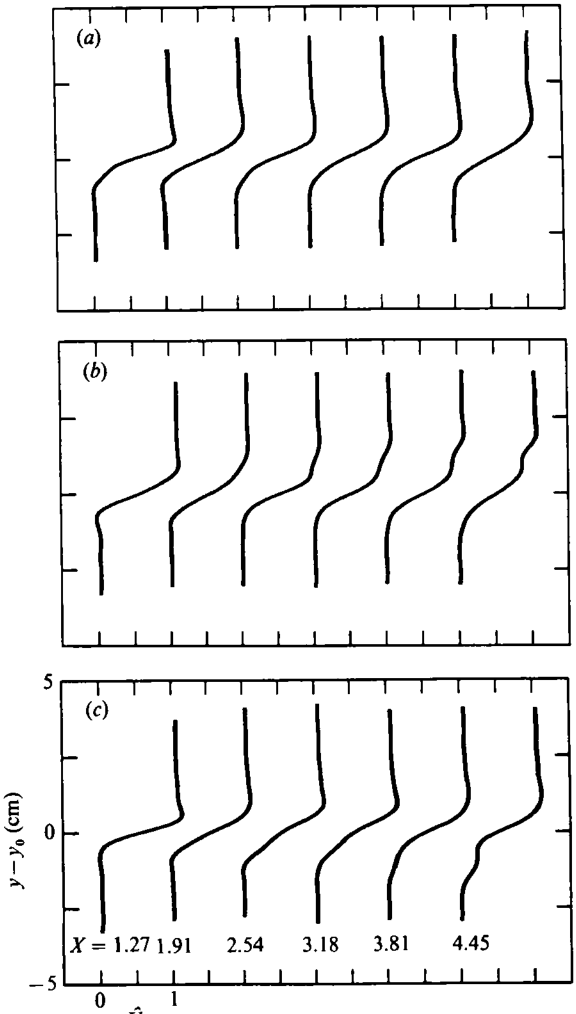

FIGURE 11. Mean streamwise velocity profiles $U(y)$ at six equally spaced streamwise stations ($5.1\ \mathrm{cm} \leqslant x \leqslant 17.8\ \mathrm{cm}$). (*a*) At midspan with spanwise-uniform excitation; (*b*) spanwise-non-uniform excitation ($\lambda_z = 2.54$ cm) at a spanwise location corresponding to the head of a streamwise vortex; (*c*) as in (*b*) but at a spanwise location corresponding to a tail. The high and low speeds of each profile are 30 and 10 cm/s, respectively. The velocity scale is shown on the horizontal axis of (*c*).

Even though spanwise-non-uniform excitation has a marked effect on the phase-averaged data close to the flow partition (cf. figure 10*b*), its effect on the approximately two-dimensional time-averaged base flow is only felt farther downstream as can be deduced from cross-stream profiles of the temporal mean of the streamwise velocity. These profiles are shown in figure 11(*a*) for spanwise-uniform excitation and figure 11(*b*, *c*) for spanwise-non-uniform excitation. The velocity profiles in figures 11(*b*) and 11(*c*) are measured at spanwise stations corresponding to passage of the head of a streamwise vortex (i.e. its downstream tip) and halfway ($\frac{1}{2}\lambda_z$) between the heads of two adjacent streamwise vortices (hereinafter referred to as the 'tail'), respectively. The velocity profiles in figure 11(*a*) are similar to those found in other investigations of mixing layers subjected to harmonic forcing

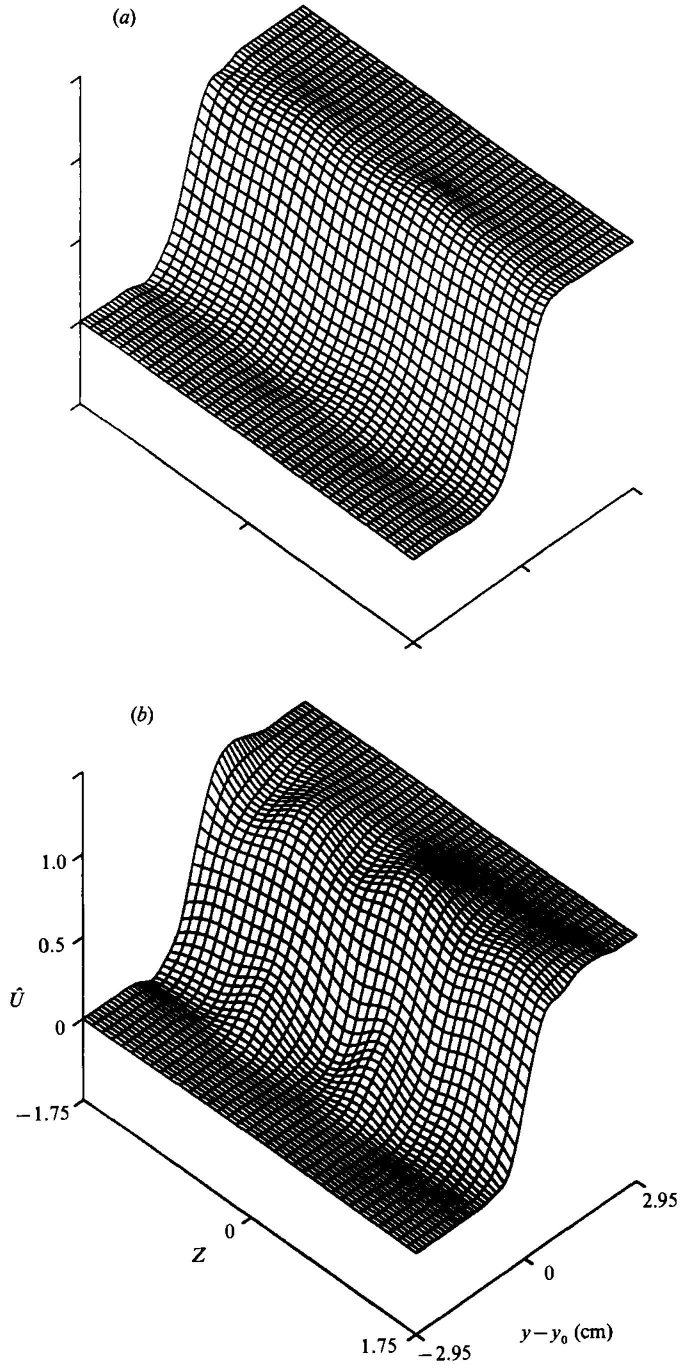

FIGURE 12. Mean streamwise velocity $U(y,z)$ at $x = 10.2$ cm. (*a*) Spanwise-uniform excitation; (*b*) spanwise-non-uniform excitation.

by other means (e.g. Weisbrot 1984). Of particular note is the development of a slight velocity overshoot (exceeding U_1) at the high-speed side, reported earlier by Gaster, Kit & Wygnanski (1985) for a mechanically forced flow. In addition to a velocity overshoot at the high-speed side, the measurements of Weisbrot reveal a velocity undershoot at the low-speed side. Streamwise velocity overshoot (or undershoot) on the high-speed (or low-speed) edge of the mixing layer may lead to a significant diminution in the momentum thickness, even though the width of the mixing layer (as measured by the presence of vorticity) does not necessarily decrease. To the extent that streamwise derivatives of the time-averaged cross-stream velocity component in a two-dimensional mixing layer are small compared to $\partial U/\partial y$ (e.g. Townsend 1980), the mean spanwise vorticity ω_z of the flow is dominated by the latter. Hence, the velocity overshoot evident in figure 11(*a*) may mark the appearance of (small) negative values of ω_z on the high- and low-speed edges of the mixing layer. Although negative spanwise vorticity may also be present in the unforced flow, its mean magnitude is likely to be considerably smaller owing to substantial variation among the cross-stream widths of the primary vortices.

When the excitation waveform is spanwise-non-uniform, the mean velocity profiles distort downstream. Because the (approximately) streamwise vortices in the braid region are inclined in the (x, y)-plane, the profiles in figure 11(*b*, *c*) are most strongly affected near their high- and low-speed edges, respectively. Furthermore, since the streamwise vortical structures have their origin in hairpin eddies which form on the high-speed side of the spanwise vortices (figure 7*f*), the mean profiles are first distorted near the high-speed edge. Because 'localized' inflexion points of the distorted mean velocity profiles mark regions of large shear, their appearance has important consequences from the standpoint of mixing transition. These regions are associated with thin internal shear layers, in which the growth rate of small disturbances is proportional to the local rate of strain and inversely proportional to the shear-layer thickness (Landahl & Mollo-Christensen 1986). The rapid amplification of these small-scale disturbances is similar to the inviscid instability observed by Klebanoff, Tidstrom & Sargent (1962) in a transitional boundary layer.

Distortion of the streamwise velocity profiles due to spanwise-non-uniform excitation is not restricted to the cross-stream (x, y)-plane. Surfaces of mean streamwise velocity are also deformed in the (y, z)-plane (figure 12*a*, *b* for $x =$ 10.2 cm, and figure 13*a*, *b* for $x =$ 17.8 cm). Spanwise-uniform excitation results in a reasonably two-dimensional distribution of the mean streamwise velocity at $x =$ 10.2 cm, while at $x = 17.8$ cm some non-uniformity associated with 'natural' evolution of three-dimensional flow structures is developed. The disturbances leading to these flow structures are most likely associated with imperfections in the experimental apparatus. The respective Reynolds numbers based on the spanwise-averaged momentum thickness $\Theta(x)$ are 340 and 570. When the excitation waveform is spanwise-non-uniform, the temporal mean streamwise velocity distribution develops trough- and ridge-like distortions aligned in the y-direction, and alternating in z with the spanwise wavelength of the excitation waveform. Distortion of the mean streamwise velocity distribution results in a substantial increase in $\Theta(x)$ at these two streamwise locations, and consequently an increase in the respective values of $Re_{\Theta(x)}$ (490 and 950). Although this distortion is strongest along the high- and low-speed edges of mixing layer (i.e. at the heads and tails of the streamwise vortices), it is evident throughout the entire velocity surface and is accompanied by approximately spanwise-periodic inflexion points in spanwise profiles of the mean streamwise velocity at fixed y-elevations. These inflexion points suggest the formation of local maxima of spanwise strain rate and rapid amplification of small disturbances, as does the distortion of the cross-stream profiles. The breakdown of these rapidly amplifying structures leads to generation of small-scale turbulence. The formation of localized shear layers by interaction among the streamwise and primary

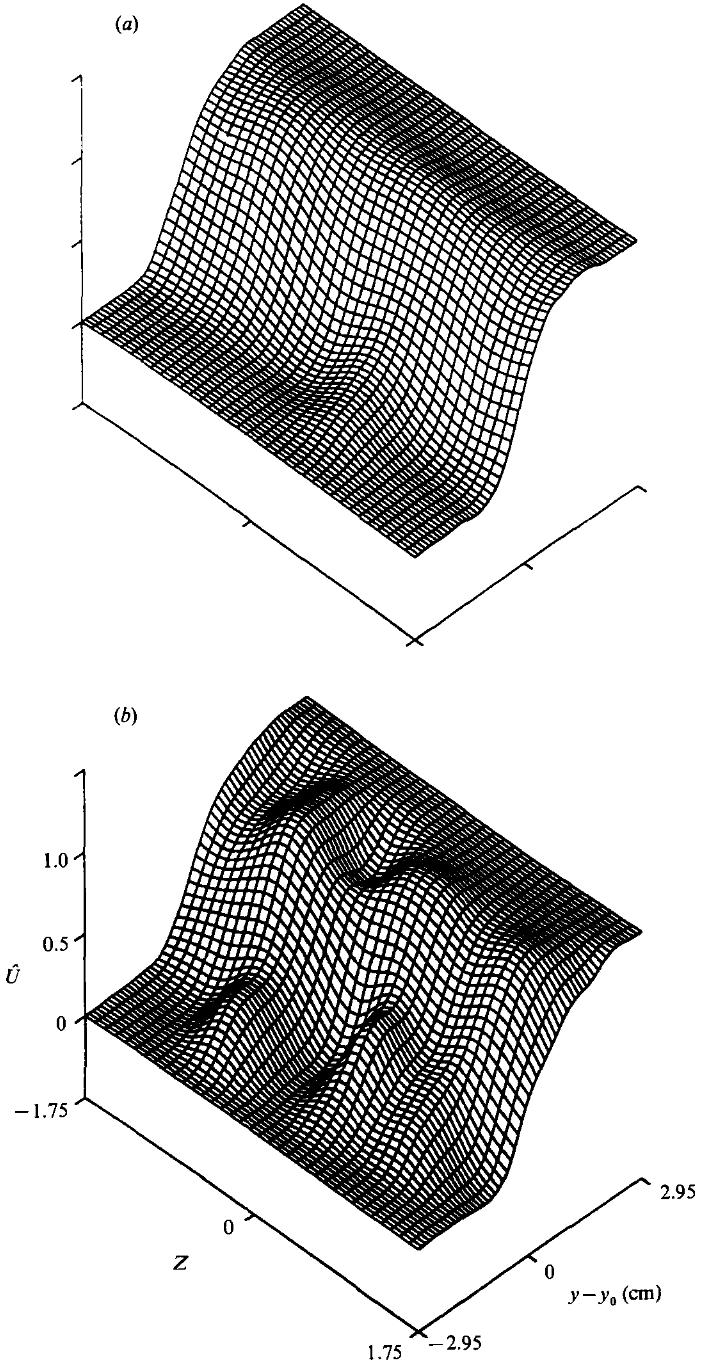

FIGURE 13. As for figure 12, with $x = 17.8$ cm.

vortices is also suggested by Corcos (1988). Such shear layers may be formed by the wrapping of spanwise vortex lines around cores of streamwise vortices.

The role of streamwise vortices in the formation of spanwise concentrations of small-scale flow structures is demonstrated in spanwise contour plots of velocity power spectra $P(z, \nu)$ (figure 14 at $x = 10.2$ cm, and figure 15 at $x = 17.8$ cm). These

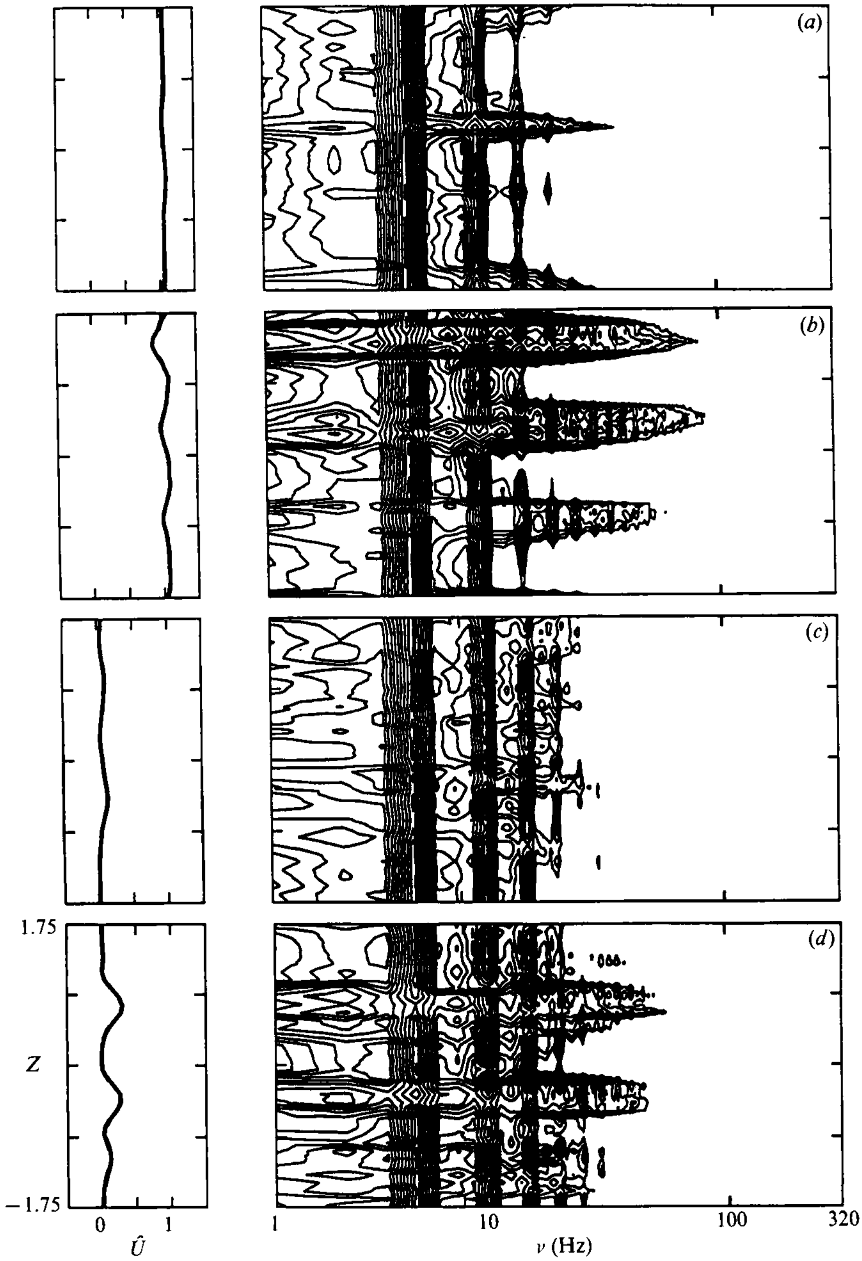

FIGURE 14. Contours of $P(z,\nu)$ at $x = 10.2$ cm and at two y-elevations of inflexion points of $U(y)$ which result from spanwise-non-uniform excitation (cf. figure 11*b*, *c*). (*a*) Spanwise-uniform excitation, at $y-y_0 = 1.1$ cm (close to high-speed side); (*b*) spanwise-non-uniform excitation, at $y-y_0 = 1.1$ cm; (*c*) spanwise-uniform excitation, at $y-y_0 = -0.70$ cm (close to low-speed side); (*d*) spanwise-non-uniform excitation, at $y-y_0 = -0.70$ cm. Spanwise distributions of mean streamwise velocity are shown to the left of each contour plot. Contour increments are logarithmic, starting at 10^{-3} cm^2/s^2. The ratio of consecutive contour levels is $10^{0.25}$.

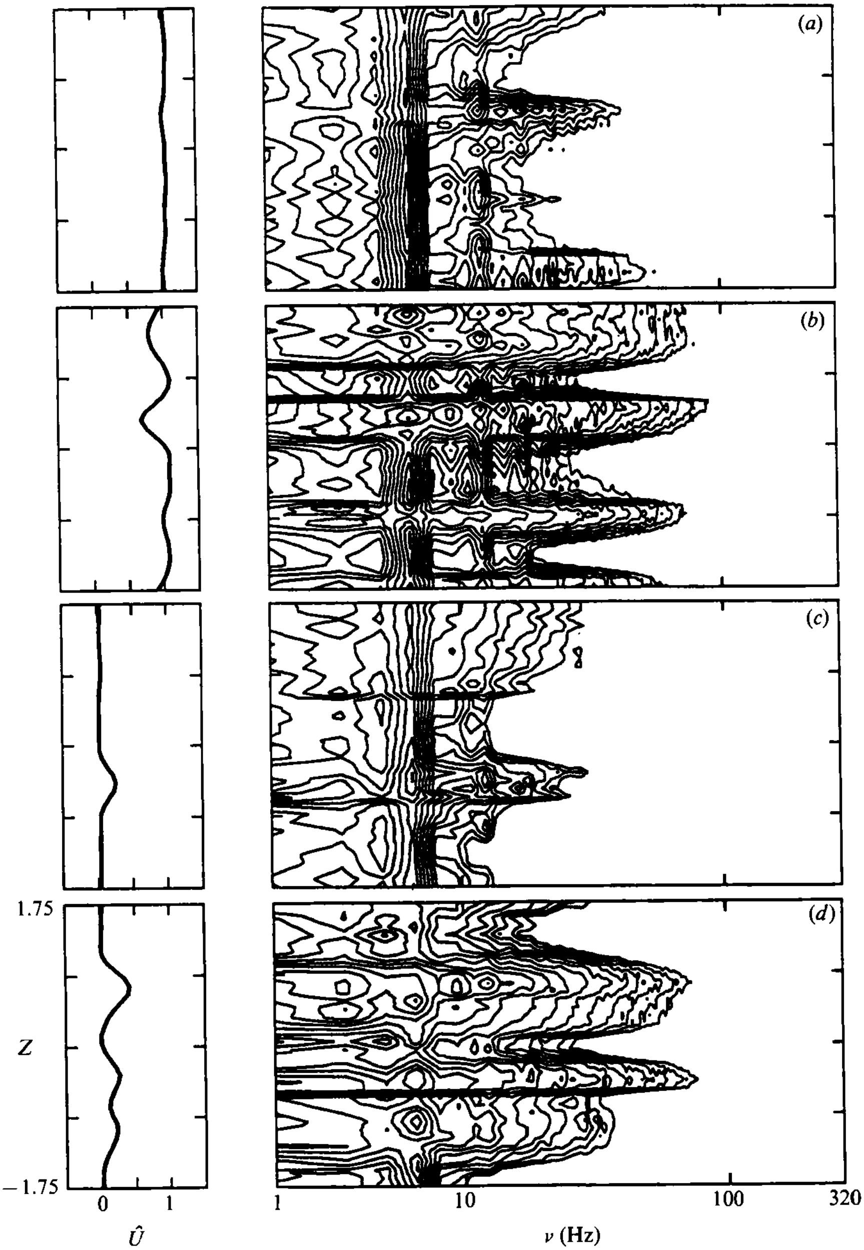

FIGURE 15. As for figure 14, with $x = 17.8$ cm. (a) $y-y_0 = 1.5$ cm; (b) $y-y_0 = 1.5$ cm; (c) $y-y_0 = -1.4$ cm; (d) $y-y_0 = -1.4$ cm.

data are plotted at y-elevations of the inflexion points on the high- and low-speed edges of the mean cross-stream velocity profiles which result from spanwise-non-uniform excitation (cf. figure 11*b, c*). Corresponding spectra for spanwise-uniform harmonic excitation are shown for comparison in figures 14(*a, c*) and 15(*a, c*). The spanwise profile of the mean streamwise velocity at the y-elevation of each contour plot is shown to the left.

Bands of high-frequency spectral components which are approximately spanwise-

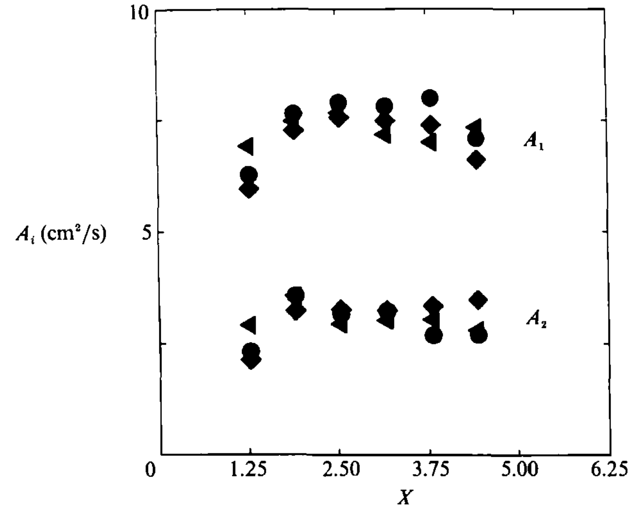

FIGURE 16. Cross-stream integrated amplitudes of the spectral components of $\langle u_{pert}(\boldsymbol{x}, t)\rangle$ at the forcing frequency (A_1) and its first harmonic (A_2). ●, Spanwise-uniform excitation at midspan; spanwise-non-uniform excitation at spanwise locations corresponding to the head (◀) and a tail (◆) of a streamwise vortex (cf. figure 11).

periodic form when the flow is subjected to spanwise-non-uniform excitation. These bands are centred around spanwise extrema of U, and the sharp spanwise gradients along their edges approximately coincide with spanwise inflexion points of U (figures 14*b*, *d* and 15 *b*, *d*). Note that the spanwise positions of the bands near the high- and low-speed edges of the mixing layer are offset by $\frac{1}{2}\lambda_z$, as are the heads and tails of the streamwise vortices. The formation of these bands near the inflexion points suggests that the inflexion points play an important role in the generation of high-frequency small-scale motion. Furthermore, at the spanwise locations of the bands, the amplitude of the spectral components at the excitation frequency ν_f and its first harmonic $2\nu_f$ undergo considerable attenuation between $x = 10.2$ cm and 17.8 cm, indicating (spanwise-non-uniform) energy transfer from low to high frequencies. This process is accompanied by a substantial reduction in the amplitude of higher harmonics of the excitation frequency. A similar trend is apparent in the streamwise variation of the power spectra of streamwise velocity in an unforced mixing layer undergoing small-scale transition (Huang & Ho 1990).

Cross-stream integrated amplitudes of the spectral components of $\langle u_{pert}(\boldsymbol{x}, t)\rangle$ at the forcing frequency and its first harmonic, denoted by A_1 and A_2, respectively, are shown in figure 16 for spanwise-uniform and spanwise-non-uniform excitation (cf. figures 11*a–c*). To the extent that the local slope of each curve is a measure of local streamwise amplification rate (cf. e.g. Gaster *et al.* 1985), the value of x at which the slope vanishes is the location of zero spatial amplification. When the flow is excited by a spanwise-uniform wavetrain, A_1 increases somewhat between $x = 5.1$ cm ($X = 1.27$) and 7.6 cm ($X = 1.90$), and then remains almost unchanged until $x = 15.2$ cm ($X = 3.80$), where it begins to decay (except possibly at the head location). The second harmonic content of $\langle u_{pert}(\boldsymbol{x}, t)\rangle$ for the case of spanwise-uniform excitation is indicative of nonlinear behaviour of two-dimensional spanwise vortices. It is remarkable that when the flow is subjected to spanwise-non-uniform excitation, streamwise distributions of A_1 and A_2 at spanwise locations of the heads and tails of the streamwise vortices are quite similar to corresponding amplitude distributions under spanwise-uniform excitation. This suggests that, at least within the streamwise domain considered here, the evolution of the nominally two-dimensional spanwise vortices is almost unaffected by spanwise-non-uniform excitation and the accompanying formation of the streamwise vortices. In view of this finding, we conclude that attenuation of spectral components at the forcing frequency and its higher harmonics is limited to the neighbourhood of spanwise inflexion points induced by spanwise-non-uniform excitation (figures 14 and 15). The direct numerical simulations of Riley *et al.* (1988) show that two-dimensional instability modes of the plane mixing layer also appear to be unaffected by three-dimensional disturbances. We note that these conclusions may not be valid if λ_z is long enough to excite the core instability (cf. figure 9*a*, *b*).

3.4. *The evolution of small-scale motion*

The phase-averaged flow structure resulting from spanwise-non-uniform excitation is studied in detail in constant-x planes at $x = 10.2$ cm and 17.8 cm. These streamwise locations are chosen because Schlieren visualization and preliminary measurements indicated that at $x = 10.2$ cm ($X = 2.55$) the streamwise vortices are fully developed, and between this station and $x = 17.8$ cm ($X = 4.45$), three-dimensionality within the spanwise vortices and in the braid region increases substantially. The data are taken on a rectangular grid measuring 8.9 cm and 5.9 cm in the spanwise and cross-stream directions, respectively.

The small-scale streamwise motions associated with the passage of large coherent vortical structures at the measurement station are studied using zone-averaged turbulent intensity:

$$\langle u'_{za}(\boldsymbol{x}, t)\rangle = \frac{u'_t(\boldsymbol{x}, t)\,\gamma(\boldsymbol{x}, t)}{\gamma(\boldsymbol{x}, t)},$$

which emphasizes structural details of interfaces (or boundaries) separating turbulent and non-turbulent fluid. The phase-averaged turbulent fluctuations of the streamwise velocity component $\langle u'_t(\boldsymbol{x}, t)\rangle$ are calculated from instantaneous velocity records using a (digital) high-pass filter (cf. §3.2). The intermittency $\gamma(\boldsymbol{x}, t)$ identifies turbulent structures in terms of the presence or absence of small-scale fluctuations in space or time. In the present experiments the temporal intermittency is computed pointwise from the streamwise velocity $u(\boldsymbol{x}, t)$ using the procedure of Glezer & Coles (1990). The local r.m.s. deviation $\epsilon(\boldsymbol{x}, t)$ from a least-squares straight-line fit of three data points in the time series $u(\boldsymbol{x}, t)$ is computed for the middle point and compared with a prescribed threshold. If $\epsilon(\boldsymbol{x}, t)$ exceeds the threshold, the flow is called turbulent and the intermittency is set to unity at the middle point; otherwise, it is set to zero. The result is a time series $\gamma(\boldsymbol{x}, t)$ of ones and zeros. The ensemble-averaged intermittency $\langle\gamma(\boldsymbol{x}, t)\rangle$ varies between zero and one, and may be thought of as a measure of the probability that the flow is turbulent. Zone-averaged flow quantities are normally biased towards (and hence emphasize) flow features near turbulent boundaries, characterized by low values of $\langle\gamma\rangle$. The values of the zone-averaged u', where $\langle\gamma\rangle \approx 1$, are approximately equal to $\langle u'_t\rangle$. Although u' and γ vanish outside turbulent regions, in the present manuscript $\langle u'_{za}\rangle$ is calculated only for $\langle\gamma\rangle \geqslant 0.005$.

Figure 17(*a–c*) shows contour plots of $\langle u'_t\rangle$, $\langle\gamma\rangle$, and $\langle u'_{za}\rangle$ at $x = 10.2$ cm, in the (y, t)-plane for spanwise-uniform excitation. At this measurement station, passage of the spanwise vortex can be recognized by concentrations of small-scale velocity fluctuations in a relatively small region closer to the low-speed edge of the vortex (figure 17*a*). The cross-stream intermittency distribution during passage of the spanwise vortex (figure 17*b*) has two maxima, upstream and downstream, which

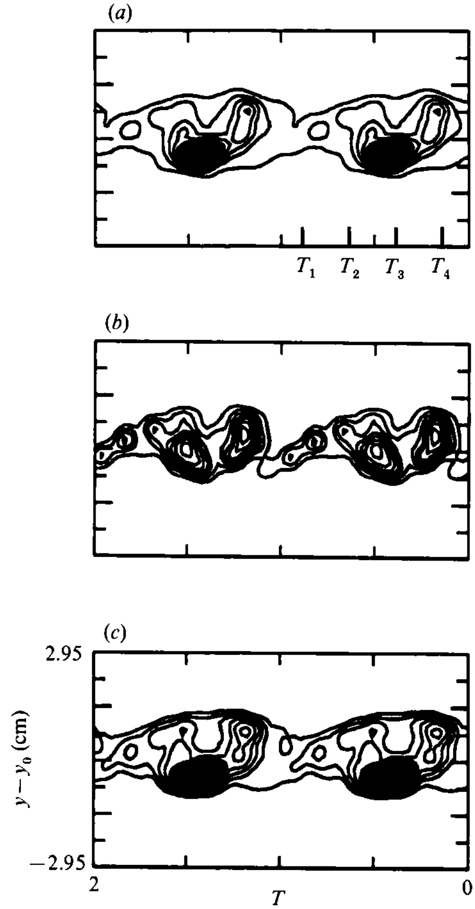

FIGURE 17. Contour plots of (*a*) turbulent intensity, (*b*) intermittency, and (*c*) zone-averaged turbulent intensity for spanwise-uniform excitation at $X = 2.55$. (*a*) $\langle u_t'(y,t)\rangle/\Delta U$ (contours start at 0.01 with contour increments of 0.01); (*b*) $\langle \gamma(y,t)\rangle$ (contours start at 0.1 with contour increments of 0.1); (*c*) $\langle u_{za}'(y,t)\rangle/\Delta U$ (contours start at 0.01 with contour increments of 0.01). The four equally spaced bold time marks correspond (from left to right) to T_1, T_2, T_3, and T_4 ($T = t/t_f$) and are for reference in figures 19, 20, and 24.

appear to be associated with entrainment of irrotational fluid from the low- and high-speed streams, respectively. Three equally spaced, weak intermittency maxima in the braid region correspond to higher harmonics in the velocity spectra (cf. figure 14*a*) and can be connected with a Kelvin–Helmholtz instability of the material interface separating the high- and low-speed fluid. Similar structures are also apparent in the numerical results of Lummer discussed by Fiedler (1988). It is noteworthy that unlike $\langle\gamma\rangle$, corresponding levels of $\langle u_t'\rangle$ in the braid region are considerably lower than within the spanwise vortices. This is because the intermittency data are sensitive to the presence of turbulent interfaces and are not a measure of turbulence intensity. Even though the base flow is nominally two-dimensional at this measurement station, the braid region is more apparent in the contour plot of the zone-averaged turbulent intensity (figure 17*c*).

That the phase-averaged structure of the base flow in the (y,t)-plane is substantially modified by spanwise-non-uniform excitation is demonstrated in contour plots of $\langle u_{za}'\rangle$ in the (y,t)-plane at $x = 10.2$ cm (figure 18*a–d*). These contour

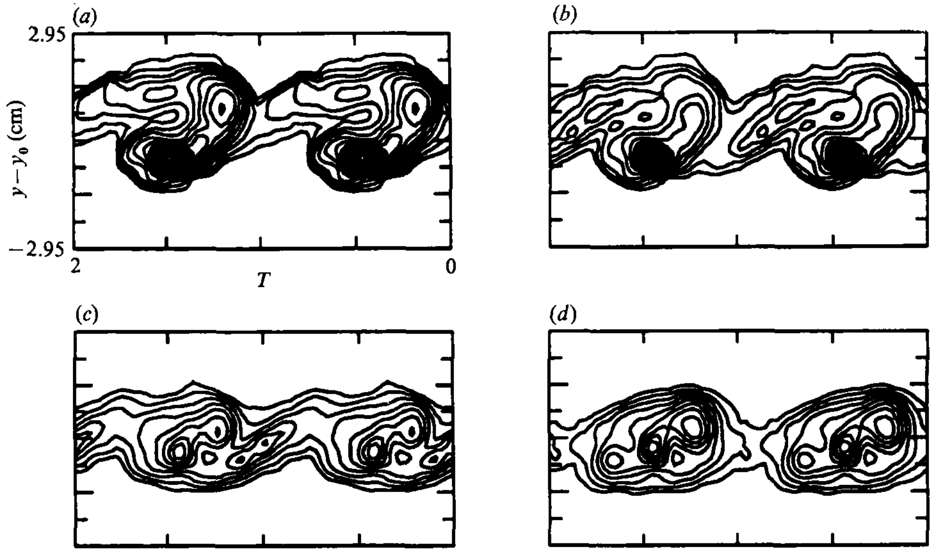

FIGURE 18. Contour plots of $\langle u_z'(y,t)\rangle/\Delta U$ at $X = 2.55$ for spanwise-non-uniform excitation at four equally spaced spanwise stations between the head (a) and tail (d) of a streamwise vortex. Contours start at 0.01, with contour increments of 0.01.

plots are cross-sections of a streamwise vortex at four equally spaced spanwise locations between its head and tail. The head of the streamwise vortex (figure 18a) appears to be separated from the spanwise vortex at the latter's upstream edge, as may be inferred from a narrow region of lower turbulence intensity between them. Note also the upstream extension (towards the braid region) of the low-speed edge of the primary vortex at the spanwise location corresponding to the tail of the streamwise vortex (figure 18d). It appears that the heads and tails of the streamwise vortices do not 'wrap' around the spanwise vortices (as suggested, for example, by the sketches of Lasheras & Choi 1988) but protrude in the downstream direction towards the braid region. As observed by Bernal & Roshko (1986), the streamwise vortices tend to move away from the spanwise vortices, i.e. towards the high- and low-speed streams. Hence, the heads (or tails) of the streamwise vortices are advected faster (or slower) than the spanwise vortices and can protrude into the downstream (or upstream) braid regions. Similar behaviour is evident in the direct numerical simulation of a temporally developing mixing layer (Rogers & Moser 1989) after pairing of the spanwise vortices.

A cross-section through a leg of the streamwise vortex (figure 18b) shows a considerable increase in turbulence intensity in the braid region. The local peak in turbulence intensity within the leg is due to its intersection with the (y,t)-plane at a small angle. The interaction between the tail of the streamwise vortex and the spanwise vortex is shown in figure 18(c, d) and is accompanied by a reduction in turbulence intensity within the core of the primary vortex. This reduction occurs at spanwise locations which approximately coincide with legs of the streamwise vortices at the low-speed edge of the primary vortex (see also figure 19g below).

The phase-averaged flow structure was also studied in (y,z)-planes at different phase delays relative to the zero crossings of the time-harmonic excitation $E(z,t)$. In each of figures 19(a)–19(h) for $x = 10.2$ cm ($X = 2.55$), and figures 20(a)–20(h) for

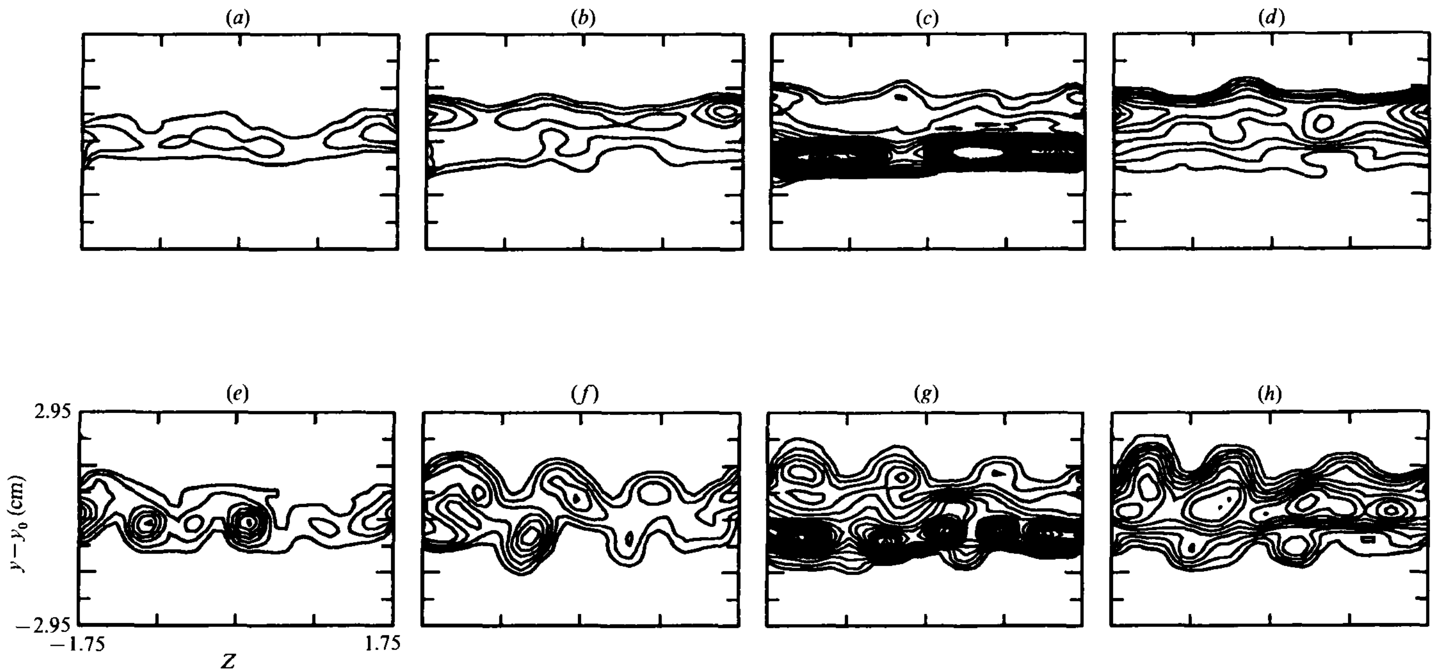

FIGURE 19. Contour plots of $\langle u'_{za}(y,z)\rangle/\Delta U$ at $x = 10.2$ cm and four evenly spaced points in time during the excitation period. (*a–d*) Spanwise-uniform excitation at T_1, T_2, T_3, and T_4, respectively; (*e–h*) spanwise-non-uniform excitation at T_1, T_2, T_3, and T_4, respectively. Contours start at 0.01, with contour increments of 0.01.

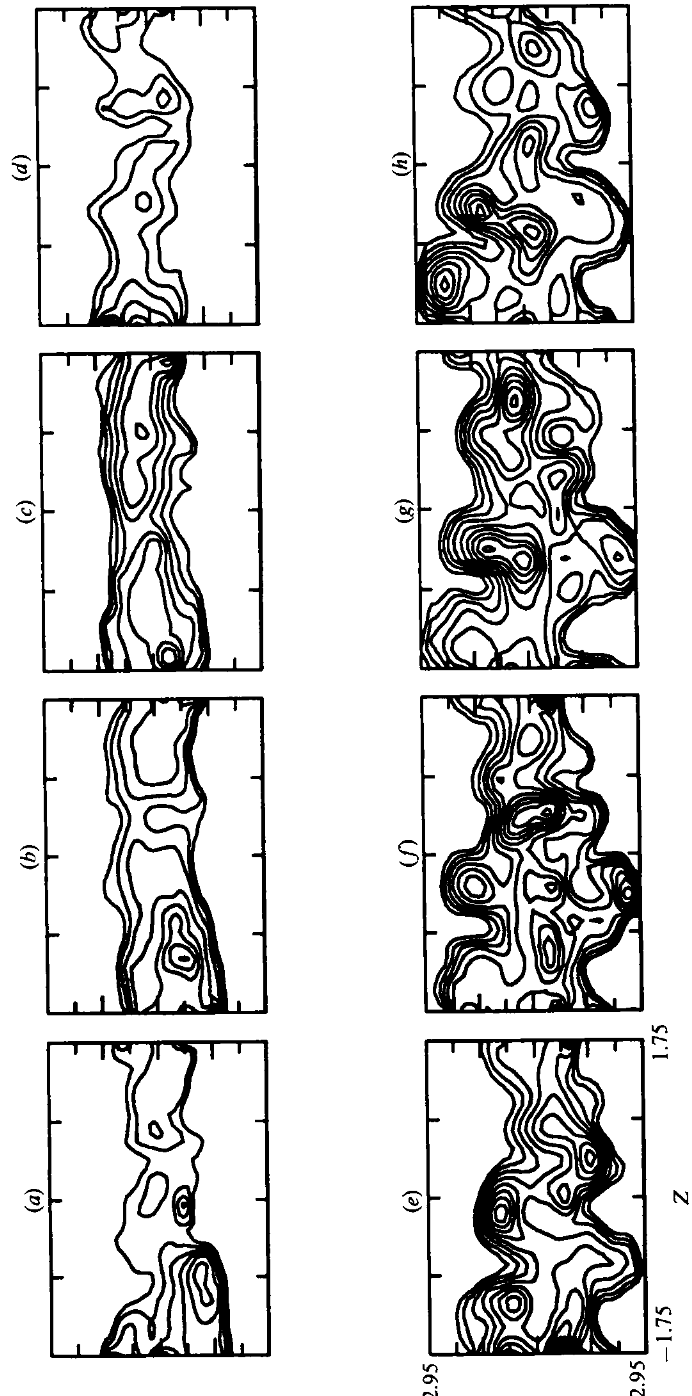

FIGURE 20. As for figure 19, with $x = 17.8$ cm.

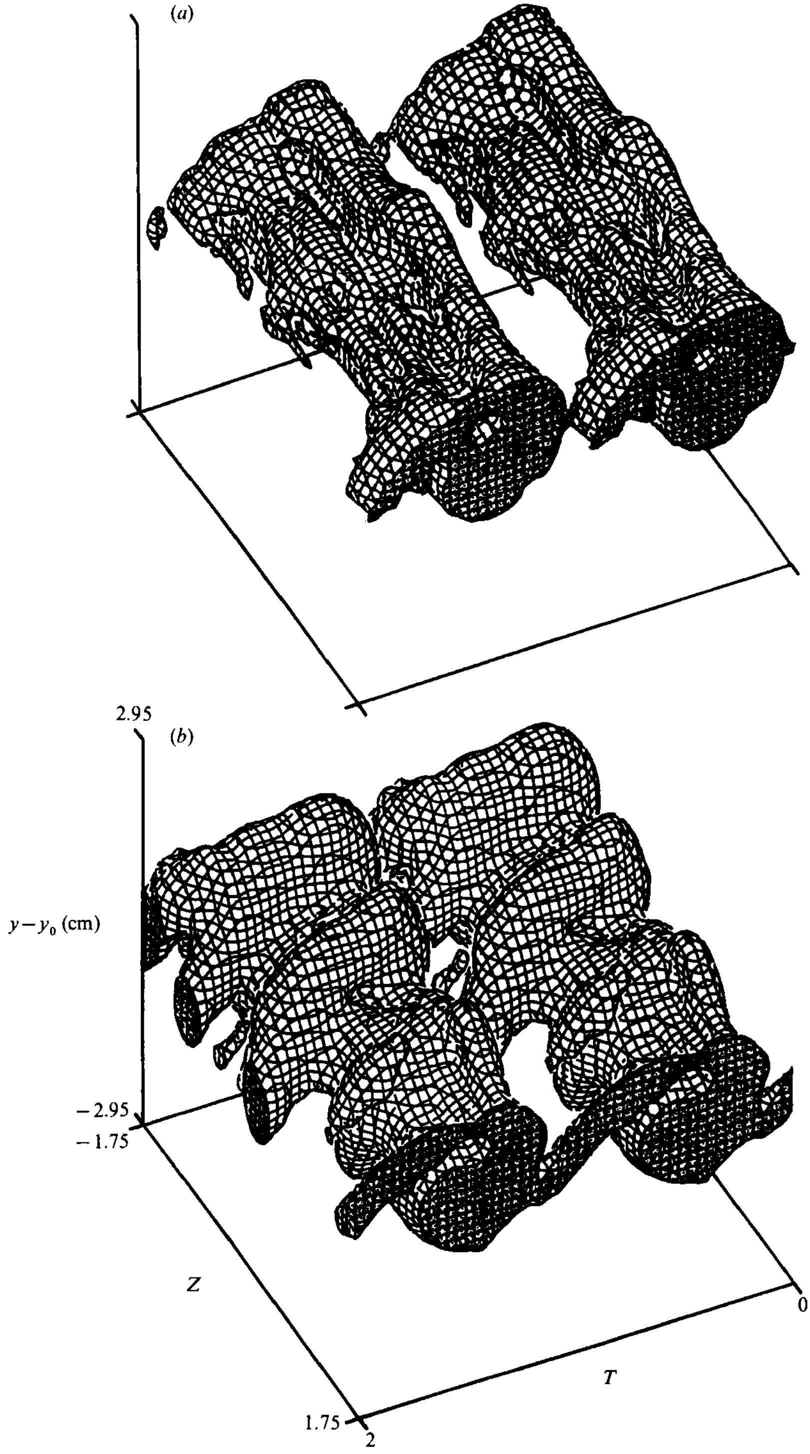

FIGURE 21. The surface $\langle u'_{za}(y,z,t)\rangle/\Delta U = 0.03$ at $x = 10.2$ cm. (*a*) Spanwise-uniform excitation; (*b*) spanwise-non-uniform excitation. Surfaces begin at $T = T_1 - \frac{1}{8}$.

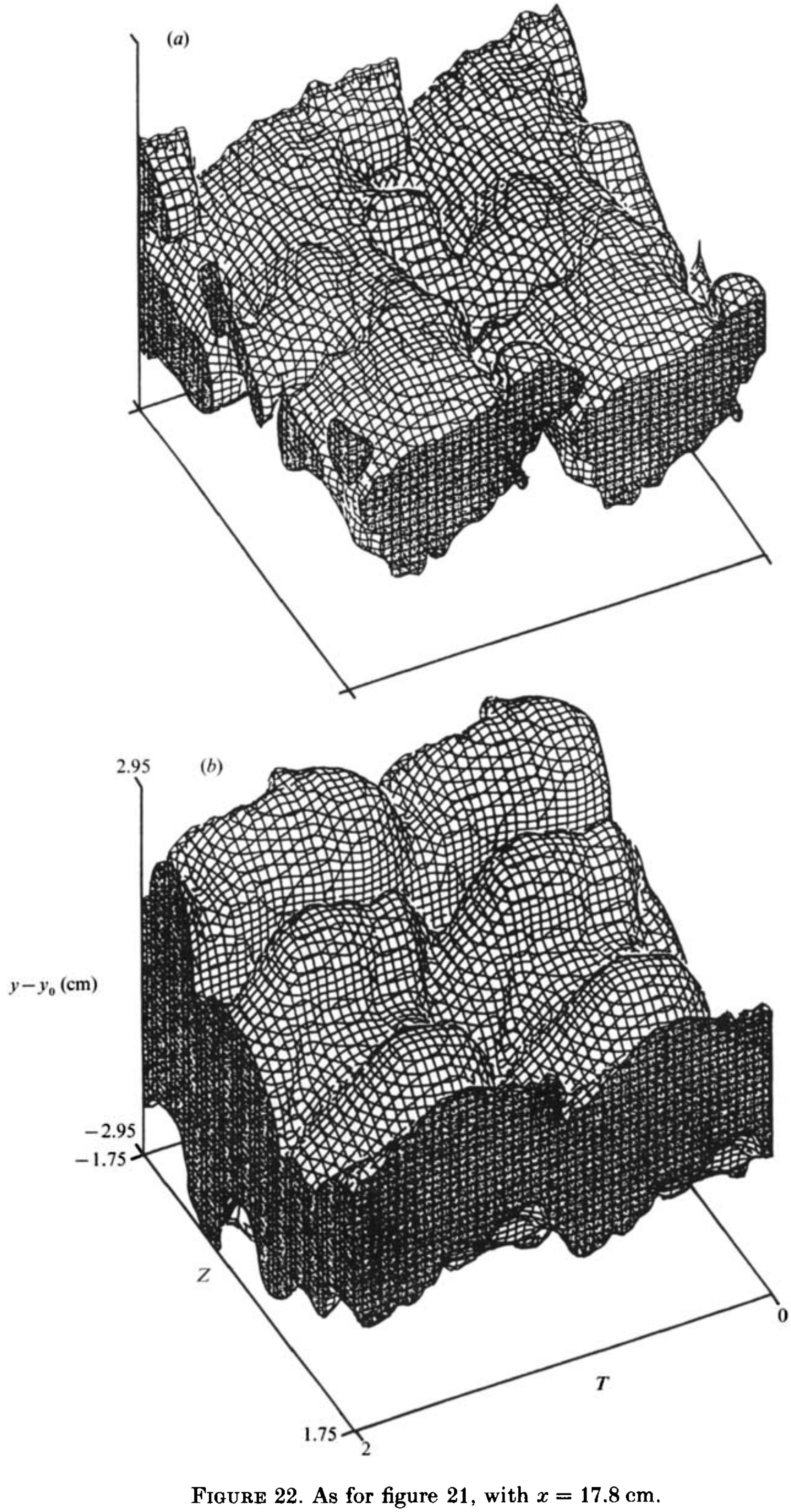

FIGURE 22. As for figure 21, with $x = 17.8$ cm.

$x = 17.8$ cm ($X = 4.45$), we show four pairs of contour plots of $\langle u'_{za} \rangle$ taken at equal time intervals during the excitation period. These times are referred to below as T_1, T_2, T_3, and T_4 ($T = t/t_f$), and are chosen so that T_1 and T_3 correspond approximately to passage of the centres of the braid region and the core of the spanwise vortex (as measured by the peak of $\langle u'_{za} \rangle$), respectively. The contour plots (*a–d*) of each figure are for spanwise-uniform excitation. Because cross-sections in the (y, z)-plane are extremely sensitive to spanwise undulations of the primary vortices, the data in figures 19 and 20 are actually plotted along lines of constant spanwise phase of the two-dimensional base flow. The necessary phase information is obtained from a (discrete) fast Fourier transform of the velocity time series measured at a y-elevation outside the mixing layer on the high-speed side (the largest spanwise phase variation is 27°).

Spanwise concentrations of zone-averaged turbulence intensity in the braid region are clearly associated with the legs of the streamwise vortices (figure 19*e*), in agreement with the observations of Breidenthal (1981). In the absence of the streamwise vortices (figure 19*a*) there is very little turbulent activity in the braid region. The (y, z)-plane at $T = T_2$ is closer to the downstream spanwise vortex, and hence the streamwise vortices are at higher y-elevations than at $T = T_1$. Furthermore, at $T = T_2$ (counter-rotating) pairs of streamwise vortices are closer to each other, indicating that the heads begin to form. We note that tails of streamwise vortices from the downstream braid region appear at the low-speed side. The heads and tails of the streamwise vortices are also apparent at the downstream edge of the spanwise vortex ($T = T_4$, figure 19*h*).

The contour plots of $T = T_3$ (figure 19*c*, *g*) represent cross-sections through the centre of the core of the spanwise vortex (as may be measured by a maximum of the turbulence intensity). Modification of the structure of the primary vortex by spanwise-non-uniform excitation is evident in the appearance of concentrations of turbulent intensity at spanwise locations of the heads of the streamwise vortices and from breakdown of the primary vortex core into spanwise-periodic concentrations of small-scale motion, having a spanwise wavelength of approximately $\frac{1}{2}\lambda_z$. The spanwise locations of these turbulence concentrations also coincide with inflexion points of the mean spanwise profile of streamwise velocity (e.g. figure 12). Furthermore, as discussed in §3.5 below, breakdown of the core is connected with the formation of approximately spanwise-periodic concentrations of all three vorticity components within the spanwise vortex as a result of its interaction with the streamwise vortices. We believe that this breakdown is a precursor to the rapid spreading of three-dimensional small-scale motion within the core of the spanwise vortex, which is necessary for mixing transition. Figure 20(*e–h*) shows that at $x =$ 17.8 cm the flow is clearly dominated by the streamwise vortices, as evidenced by strong spanwise concentrations of turbulent intensity. Of particular note is the reduction in the spanwise periodicity of the concentrations of small-scale motion within the core of the primary vortex (compare figure 20*g* to 19*g*), which suggests spanwise mixing. This evolution is accompanied by a significant increase in the cross-stream width of the mixing layer. The corresponding data for spanwise-uniform excitation (figure 20*a–d*) show less cross-stream spreading and significantly less spanwise non-uniformity within the primary vortex and the braid region.

As noted in §3.1, iso-surfaces of zone-averaged r.m.s. streamwise velocity fluctuations may be useful in studying the three-dimensional structure of the flow. Figures 21(*a*, *b*) and 22(*a*, *b*) show the surface $\langle u'_{za}(y, z, t) \rangle / \Delta U = 0.03$ at $x = 10.2$ cm and 17.8 cm, respectively, during two periods of the excitation waveform. These and the following iso-surface plots (figures 23 and 26) begin at $T = T_1 - \frac{1}{8}$, i.e. at a cross-section in the (y, z)-plane close to the centre of the braid region (cf. figure 19*a*, *e*). When the excitation is spanwise-uniform, the spanwise vortices and the braid region are approximately two-dimensional. The spanwise trough along each primary vortex separates upstream and downstream regions of concentrated velocity fluctuations, apparently connected with entrainment of high- and low-speed fluid, respectively, into the spanwise vortex. Spanwise-non-uniform excitation leads to formation of structures with substantial spanwise non-uniformity. The heads of the streamwise vortices appear on the high-speed side of the primary vortex, with spanwise spacings approximately equal to the excitation wavelength λ_z. The legs of streamwise vortices in the braid region are not all of equal strength, presumably due to spanwise variations in the strain field, which is in turn affected by the primary vortices. (As shown in figure 9, spanwise undulations of the primary vortices have a substantial effect on the evolution of the streamwise vortices.) Figure 21 (*b*) further suggests that appearance of the streamwise vortices results in substantial enlargement of turbulent interfaces into the free streams.

For spanwise-uniform excitation, figure 22 (*a*) shows that farther downstream the primary vortices have developed spanwise irregularities. These appear to be associated with formation of unforced streamwise vortices. Note the decrease in the inclination relative to the x-direction of the major axis of the nominally oval cross-section of these vortices. Because the fundamental instability mode becomes neutral where the major axis is oriented normal to the streamwise direction (roughly at $x =$ 10.2 cm in our experiments) and decays thereafter, this change has been connected by Weisbrot (1984) with spatial amplification of harmonically excited waves. For spanwise-non-uniform excitation, figure 22 (*b*) shows a substantial increase in the cross-stream width of the mixing layer (as may be defined by spreading of turbulent interfaces), although this surface does not show details of the streamwise structures. For $x = 17.8$ cm, the surface $\langle u'_{za}(y, z, t)\rangle / \Delta U = 0.055$ (figure 23) indicates that the heads and tails of the streamwise vortices protrude into the downstream and upstream braid regions, respectively. As discussed above, this protrusion is possible because the heads and tails are advected at higher and lower velocities than the high-speed and low-speed edges of the primary vortices, respectively. Figure 23 also suggests the formation of approximately toroidal regions of $\langle u'_{za}\rangle$ around the primary vortices due to upstream and downstream protrusion of the streamwise vortices (see also figure 9*d*).

3.5. *An approximation to cross-stream vorticity*

We next focus attention on the phase-averaged cross-stream component of vorticity $\langle \omega_y \rangle = \partial\langle u\rangle/\partial z - \partial\langle w\rangle/\partial x$. Assuming that all the terms in the phase-averaged continuity equation are of the same order, it may be argued that

$$\frac{\partial\langle w\rangle/\partial x}{\partial\langle u\rangle/\partial z} \sim \left(\frac{\Delta z}{\Delta x}\right)^2,$$

where $\Delta z = \frac{1}{2}\lambda_z$ and $\Delta x = \lambda_x$ are appropriate characteristic lengthscales in the spanwise and streamwise directions, respectively. In the present experiments $[(\frac{1}{2}\lambda_z)/\lambda_x]^2 \approx \frac{1}{16}$ and, hence, the ensemble-averaged cross-stream vorticity components may be approximated by $\langle \tilde{\omega}_y \rangle = \partial u(\boldsymbol{x}, t)\rangle / \partial z$. Although it is clear that this approximation makes it impossible to distinguish between vortical and irrotational distortions of the streamwise velocity profile, its use in what follows enables us to develop a three-dimensional structure of the streamwise vortices. Contours of

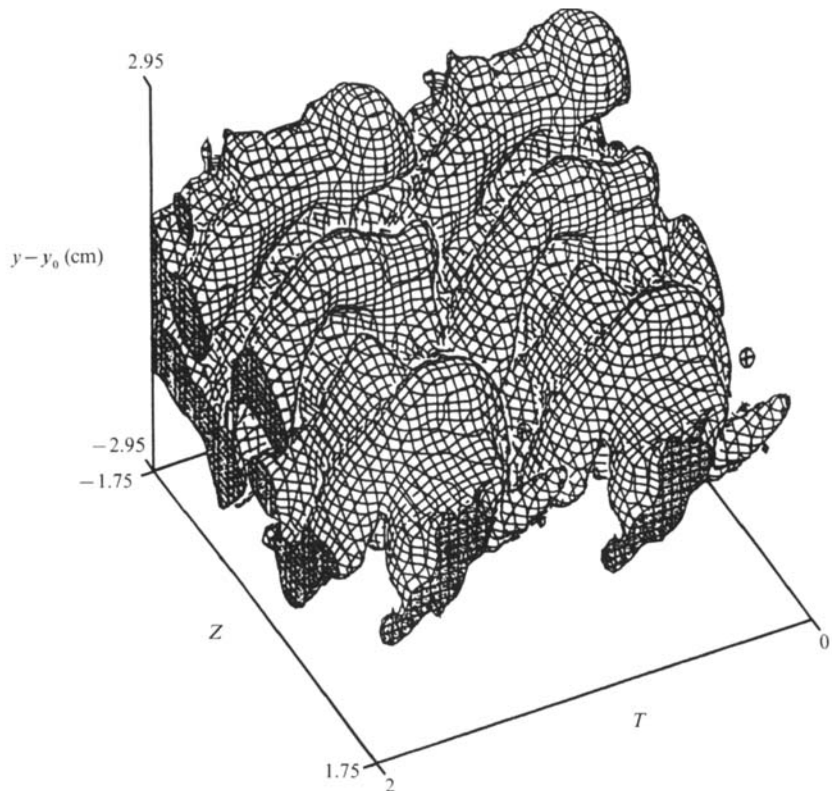

FIGURE 23. The surface $\langle u'_{za}(y,z,t)\rangle/\Delta U = 0.055$ at $x = 17.8$ cm for spanwise-non-uniform excitation. Surface begins at $T = T_1 - \frac{1}{8}$.

$\langle\tilde{\Omega}_y\rangle = \langle\tilde{\omega}_y\rangle\lambda_z/U_c$ are shown in figure 24(a–h) for $x = 10.2$ cm and figure 25(a–h) for $x = 17.8$ cm at $T = T_1$, T_2, T_3, and T_4 (cf. figures 19a–h and 20a–h). In most of the braid region, the vorticity within the streamwise vortices is likely to have two approximately equal components in the x- and y-directions (ω_x and ω_y). Thus, streamwise vortices in the (y,z)-plane at $T = T_1$ (figure 24e) may be recognized by alternating concentrations of positive and negative $\langle\tilde{\Omega}_y\rangle$, coinciding with concentrations of $\langle u'_{za}\rangle$ in figure 19(e). It should be noted that the level of $\langle\tilde{\Omega}_y\rangle$ is quite low for spanwise-uniform excitation (figure 24a). A notable feature of the results for spanwise-non-uniform excitation (figures 24e–h and 25e–h) is the downstream preservation of spanwise (and streamwise) coherence of the phase-averaged flow features. In contrast, contour plots of $\langle u'_{za}\rangle$ have less spanwise coherence at $x =$ 17.8 cm (figure 20e–h) than at $x = 10.2$ cm (figure 19e–h).

Of particular interest is the distribution of $\langle\tilde{\Omega}_y\rangle$ within the primary vortex core when the mixing layer is subjected to spanwise-non-uniform excitation. (Note for comparison the corresponding distributions for spanwise-uniform excitation in figure 24(c) for $x = 10.2$ cm and figure 25(c) for $x = 17.8$ cm.) The distribution of $\langle\tilde{\Omega}_y\rangle$ in the (y,z)-plane at $T = T_3$ (figures 24g and 25g) is comprised of three approximately regular spanwise rows, each consisting of approximately spanwise-periodic concentrations of $\langle\tilde{\Omega}_y\rangle$ of alternating signs having a wavelength $\frac{1}{2}\lambda_z$. Concentrations of $\langle\tilde{\Omega}_y\rangle$ of the same sign in the top and bottom rows occur at approximately the same z-coordinate and appear to be associated with streamwise vortices in the upstream and downstream braid regions, respectively. The middle row (within the core of the

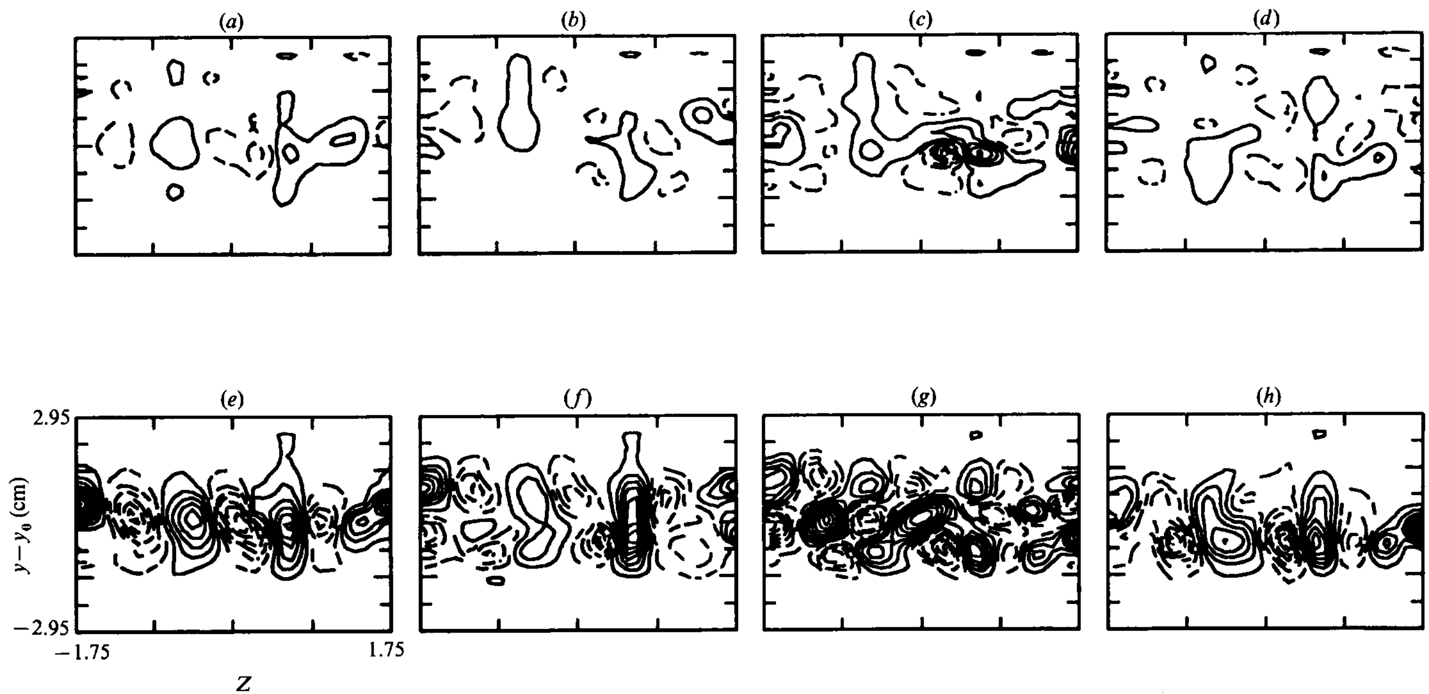

FIGURE 24. Contour plots of $\langle \tilde{\Omega}_y(y,z) \rangle$ at $x = 10.2$ cm and four evenly spaced points in time during the excitation period (as in figure 19). (*a–d*) Spanwise-uniform excitation; (*e–h*) spanwise-non-uniform excitation. Contours start at 0.1 (−0.1), with contour increments of 0.2 (−0.2). Negative contours are dashed.

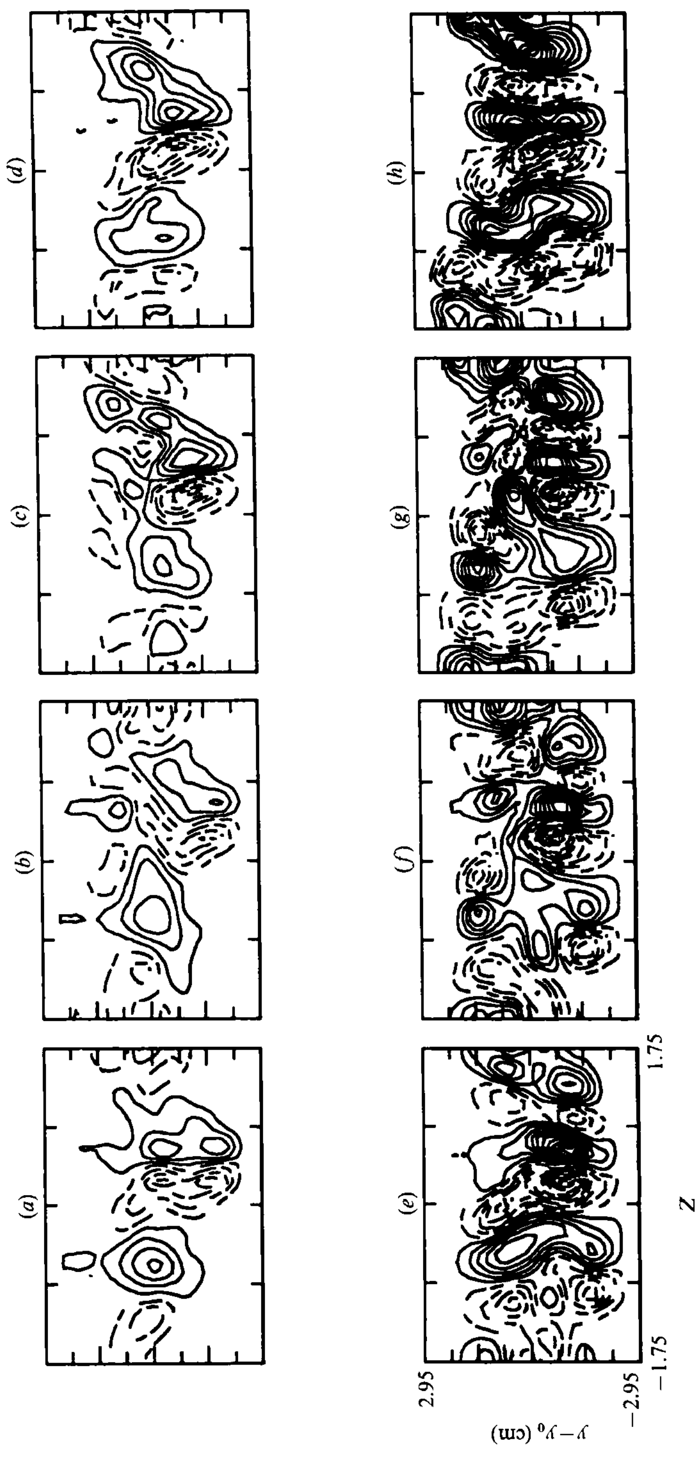

FIGURE 25. As for figure 24, with $x = 17.8$ cm.

spanwise vortex) is offset in the z-direction relative to the upper and lower rows by $\frac{1}{2}\lambda_z$.

A strikingly similar distribution of the streamwise vorticity ω_x is found in direct numerical simulations of a mixing layer (Buell & Mansour 1989) which allow for streamwise growth. The spanwise distribution of ω_x leads to spanwise-periodic intensification and weakening of the spanwise vorticity ω_z and the formation of cup-shaped concentrations. The cups form at the centre of quadrupoles comprised of four adjacent concentrations of ω_x (two in the middle row), which produce positive spanwise strain (i.e. stretching of spanwise vorticity). The spanwise locations of the resulting cups alternate above and below the middle row much like the heads and tails of the streamwise vortices. The distribution of cross-stream vorticity ω_y also has a quadrupolar structure very similar to that of figures 24(g) and 25(g) (J. C. Buell, private communication, 1990). These distributions of ω_x and ω_y within the cores of the primary vortices may result from vortex lines looping between cups. In connection with the spanwise-periodic concentrations of $\langle u'_{za}\rangle$ in figure 19(g), we note that the upper and lower cups in the results of Buell & Mansour appear at similar spanwise locations and, hence, are likely related to the spreading of small-scale motion within the core of the primary vortex.

The existence of spanwise concentrations of $\langle\tilde{\Omega}_y\rangle$ in the upper and lower rows of figures 24(g) and 25(g) may be jointly due to tilting of spanwise vortices by streamwise vortices and to the transport of cross-stream vorticity along the legs of the streamwise vortices in the upstream and downstream directions. It should be noted that axial flow along the legs of the streamwise vortices (associated with vorticity transport) can also contribute to mixing (or at least stirring) of fluid from both streams. The apparent 'tagging' of the streamwise vortices by $\langle\tilde{\Omega}_y\rangle$ allows study of their protrusion into the upstream and downstream braid regions (figure 23). Contour plots of $\langle\tilde{\Omega}_y\rangle$ at $T = T_1$ and T_4 (figure 25e, h) show vertical stacks of concentrations (pairs and triplets) of the same sign, representing cross-sections of streamwise vortices from the upstream and downstream braid regions. As mentioned in §3.4, the numerical results of Rogers & Moser (1989) show that (after pairing of two primary vortices is completed) streamwise vortices are stretched beyond the upstream and downstream spanwise vortices and towards the respective upstream and downstream braid regions. Contours of $\partial\langle v\rangle/\partial z$ in the braid region (approximately $\langle\omega_x\rangle$) measured by Huang & Ho (1990) show the appearance of cross-stream (vertical) pairs of concentrations of ω_x. Those data were obtained downstream of the first rollup of the primary vortices, and the authors remarked that the formation of streamwise vortices began immediately downstream of the flow partition.

Given the qualitative agreement between our measurements and the numerical results of Buell & Mansour (1989) and Rogers & Moser (1989), we believe that even though $\langle\tilde{\Omega}_y\rangle$ is only an approximation for the cross-stream vorticity component, it is nevertheless useful in marking the streamwise vortices. Figures 26(a, b) shows plots of the surface $\langle\tilde{\Omega}_y(y,z,t)\rangle = 0.5$ at $x = 10.2$ and 17.8 cm (cf. figures 21b and 22b). At $x = 10.2$ cm, the legs of the streamwise vortices in the braid region are unmistakable. Although the primary vortices are not immediately visible here, they can be identified by the curvature of the nearby streamwise vortices and by spanwise concentrations of $\langle\tilde{\Omega}_y\rangle$ (figure 24g). At $x = 17.8$ cm, the protrusion of streamwise vortices at some spanwise locations gives the appearance of a 'cat's-eye'-like surface around the primary vortex. In the braid region, this surface is comprised of the 'local' streamwise vortex, as well as streamwise vortices from the upstream and

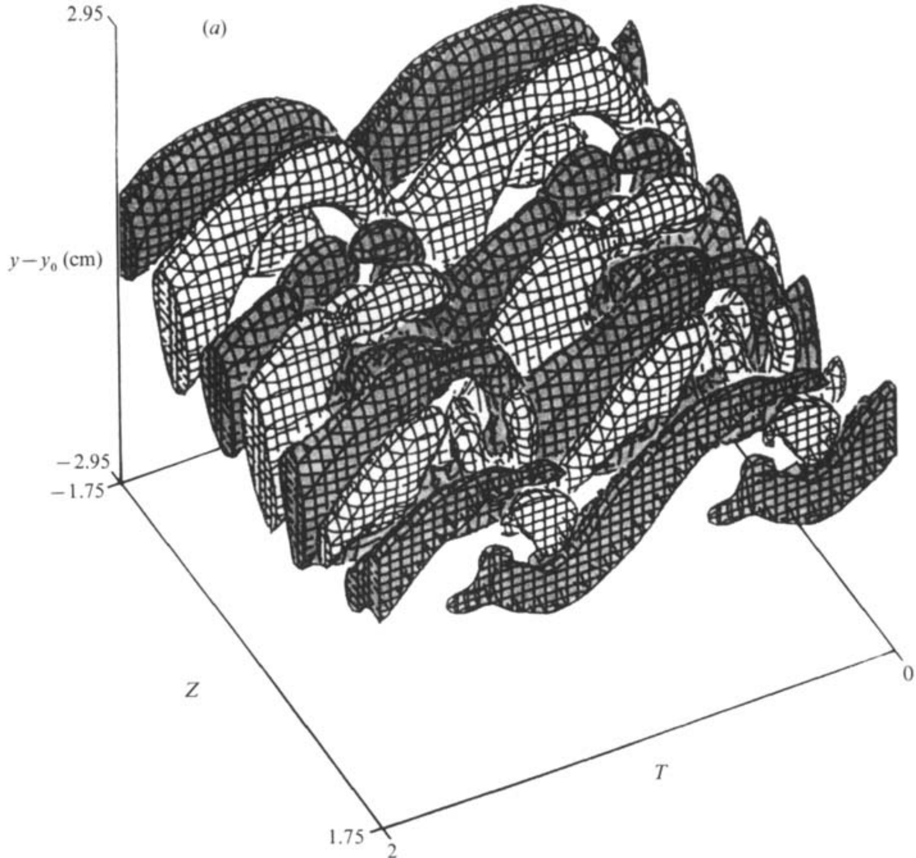

FIGURE 26. For caption see facing page.

downstream braid regions. A cross-section of this structure in the (y, t)-plane (at $x =$ 17.8 cm, $z = -1.3$ cm) is shown in figure 27. At this spanwise location the 'cat's-eye' structure is already apparent at the high-speed edge, while the leg of the streamwise vortex at the low-speed edge is stretched in the upstream direction. A vertical stack of three streamwise vortices in the braid region can also be identified at some spanwise locations in contour plots of $\langle \tilde{\Omega}_y(y, z, t) \rangle$ (figure 25*e*) and, as mentioned above, is also evident in the numerical results of Rogers & Moser.

4. Concluding remarks

Previous investigations have demonstrated that an unforced plane mixing layer is extremely receptive to small perturbations originating upstream of the flow partition. These perturbations result in spanwise concentrations of streamwise and cross-stream vorticity downstream of the flow partition and, subsequently, in the formation of streamwise vortices bearing considerable resemblance to lambda vortices in a transitional boundary layer. In the present investigation, streamwise vortices are induced by a time-harmonic heat input having a spanwise-periodic amplitude distribution, using a mosaic of surface film heaters flush-mounted on the flow partition. The streamwise vortices form downstream of the flow partition, but

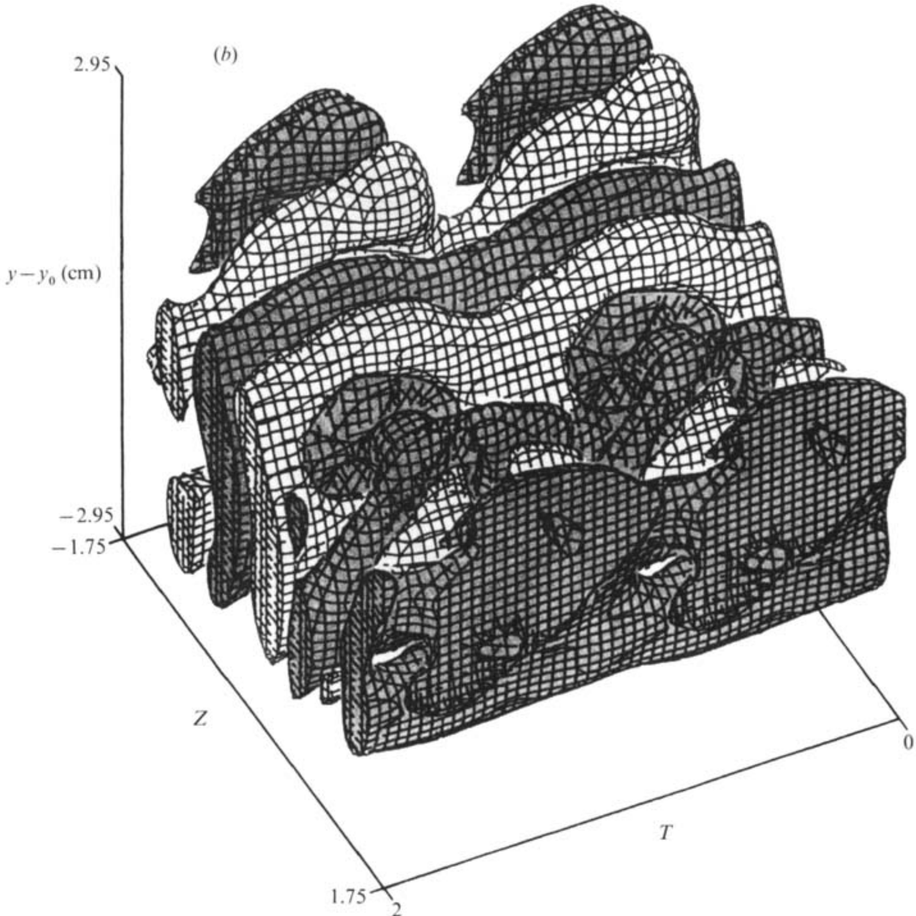

FIGURE 26. The surfaces $\langle \tilde{\Omega}_y(y,z,t) \rangle = 0.5$ (dark) and -0.5 for spanwise-non-uniform excitation. (*a*) $x = 10.2$ cm; (*b*) $x = 17.8$ cm. Surfaces begin at $T = T_1 - \frac{1}{8}$.

upstream of the first rollup of the primary vortices, presumably due to cross-stream shear and the nominally two-dimensional wave-like motion of the vorticity-containing layer between the two streams. Following the rollup of the primary vortices, the streamwise vortices reside in the braid region between consecutive primary vortices.

We have found that, for a given excitation frequency, virtually any spanwise wavelength λ_z synthesizable by the heating mosaic can be excited and can lead to formation of streamwise vortices. When the excitation wavelength is smaller than the initial wavelength of the Kelvin–Helmholtz instability, λ_{KH}, the streamwise vortices become narrower with decreasing λ_z, due to spanwise interactions. At longer excitation wavelengths the streamwise vortices become nearly isolated in the spanwise direction, and their shape appears to be wavelength-independent. In connection with these results, it is important to recognize that in all laboratory facilities, spanwise-non-uniform vorticity distributions are transported through boundary layers on the flow partition and may undergo amplification or decay. Hence, the receptivity of these boundary layers is inherently coupled to that of the ensuing shear layer. Furthermore, the sensitivity of the plane mixing layer (and the

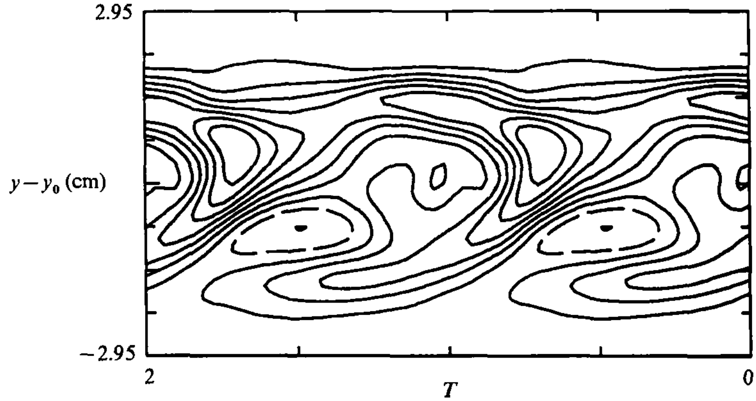

FIGURE 27. Contour plots of $\langle\tilde{\Omega}_y(y,t)\rangle$ at $x = 17.8$ cm, $z = 2.9$ cm. Contours start at 0.1 (−0.1), with contour increments of 0.2 (−0.2). Negative contours are dashed.

upstream boundary layers) to spanwise-isolated disturbances suggests that the streamwise growth of streamwise vortices is the result of a localized, rather than a global, spanwise instability mechanism.

The spanwise excitation wavelength has a profound effect on the primary vortices. When λ_z exceeds λ_{KH}, the primary vortices develop spanwise undulations persisting throughout the streamwise domain of the present observations. These undulations appear to be associated with a (translative) core instability of the primary vortices. Because the strain field within the braid region is dominated by the adjacent spanwise vortices, these undulations are accompanied by an increase in the spread angle of the streamwise vortices, and the appearance of additional vortex tubes along their legs. When $\lambda_z < \lambda_{KH}$, the spanwise vortices appear to be stable (as may be judged by the absence of spanwise undulations) to upstream disturbances which lead to the formation of streamwise vortices. We note, however, that the effect of these disturbances on the vorticity distribution within the spanwise vortices cannot be assessed owing to the interaction among the streamwise and spanwise vortices.

An important objective of the present experiments has been the identification of a mechanism which, following the appearance of streamwise vortices, leads to the generation of small-scale motion and possibly to mixing transition. We have found the appearance of streamwise vortices to be accompanied by significant distortions in distributions of mean streamwise velocity. These distortions have the shape of troughs and ridges aligned in the cross-stream direction, alternate at the excitation wavelength λ_z, and are strongest at the high- and low-speed edges of the mixing layer (i.e. at the heads and tails of the streamwise vortices). These distortions result in spanwise-periodic inflexion points not present in corresponding velocity distributions of the unforced flow. Inflexion points of the mean velocity distribution indicate the formation of locally unstable regions of large shear in which broadband perturbations already present in the base flow undergo rapid amplification and breakdown to small-scale motion. Velocity spectra at cross-stream elevations of the inflexion points develop spanwise-periodic bands of high-frequency spectral components centred around the heads and tails of the streamwise vortices.

As a result of interaction with the streamwise vortices, the primary vortices develop spanwise-periodic concentrations of small-scale motion having a spanwise wavelength of approximately $\frac{1}{2}\lambda_z$ within their cores (figure 19). We believe that this breakdown of the cores of the primary vortices is a precursor to mixing transition because farther downstream, corresponding distributions of small-scale motion have less spanwise coherence (figure 20). We note that this loss of coherence does not affect other phase-averaged quantities, such as velocity perturbations. The establishment of spanwise-periodic concentrations of small-scale motion is probably associated with the inflexional instability of the mean streamwise velocity distribution discussed above, because such instability at the low- and high-speed edges of the mixing layer leads to spanwise-periodic entrainment variations. Furthermore, these inflexion points are presumably related to spanwise-periodic concentrations of all three vorticity components within the spanwise vortices. The evolution of these vorticity concentrations has been discovered by direct numerical simulation (e.g. Buell & Mansour 1989), and their presence in the flow can also be deduced from the present data. The numerical simulations predict the formation of cup-shaped concentrations of spanwise vorticity, the spanwise locations of which almost coincide with concentrations of small-scale motion in the present data. The apparent connection between spanwise concentrations of small-scale motion and the changes in the vorticity field are indicative of the mechanisms which precede the onset of mixing transition.

Finally, the research described here utilizes a nominally two-dimensional base flow in which pairing of the primary vortices is inhibited by means of spanwise-uniform harmonic excitation. Experimental results in an unforced mixing layer (e.g. Huang & Ho 1990) suggest that small-scale transition occurs only after the first pairing of the spanwise vortices. Because our findings indicate that mixing transition in a plane shear layer subjected to spanwise-non-uniform excitation may be possible in the absence of pairing, we have recently begun to investigate the effect on the generation of small-scale motion of pairing of the primary vortices accomplished by periodic excitation at the natural frequency and its first subharmonic. The evolution of small-scale motion is being studied in the presence and absence of streamwise vortices.

The authors wish to acknowledge a number of valuable discussions with Professors F. K. Browand, H. E. Fiedler, C.-M. Ho, M. T. Landahl, W. C. Reynolds, and A. Roshko, and Dr J. C. Buell. The authors are particularly grateful to Professor H. E. Fiedler for his generous assistance in the design and construction of the Schlieren system and the traversing mechanism described in this manuscript. Some parts of the shear layer facility were constructed at the Technical University of Berlin and at Tel Aviv University; the assistance of Professors Fiedler and I. J. Wygnanski, and of The University of Arizona Engineering Experiment Station, in making these components available in 1984, is also acknowledged. Finally, the authors wish to thank Professor A. J. Pearlstein for his careful reading and comments regarding earlier versions of the manuscript.

This work has been supported by AFOSR Grants 86-0324 and 88-0271 monitored by Dr J. M. McMichael. Partial support was also provided by NSF Engineering Research Initiation Grant MSM-8505234 and through the NASA Graduate Student Researchers Program (Grant NGT-50076).

REFERENCES

Ashurst, W. T. & Meiburg, E. 1988 Three-dimensional shear layers via vortex dynamics. *J. Fluid Mech.* **189**, 87–116.

Batchelor, G. K. 1953 *The Theory of Homogeneous Turbulence*. Cambridge University Press.

Bell, J. H. & Mehta, R. D. 1989 Three-dimensional structure of plane mixing layers. *Joint Institute of Aeronautics and Acoustics Rep. TR-90.* NASA Ames Research Center.

Bernal, L. P. 1981 The coherent structure of turbulent mixing layers. I. Similarity of the primary vortex structure. II. Secondary streamwise vortex structure. Ph.D. thesis, California Institute of Technology.

Bernal, L. P. & Roshko, A. 1986 Streamwise vortex structure in plane mixing layers. *J. Fluid Mech.* **170**, 499–525.

Breidenthal, R. E. 1981 Structure in turbulent mixing layers and wakes using a chemical reaction. *J. Fluid Mech.* **109**, 1–24.

Browand, F. K. & Troutt, T. R. 1980 A note on spanwise structure in the two-dimensional mixing layer. *J. Fluid Mech.* **97**, 771–781.

Browand, F. K. & Troutt, T. R. 1985 The turbulent mixing layer: geometry of larger vortices. *J. Fluid Mech.* **158**, 489–509.

Brown, G. L. & Roshko, A. 1974 On density effects and large structure in turbulent mixing layers. *J. Fluid Mech.* **64**, 775–816.

Buell, J. C. & Mansour, N. N. 1989 Asymmetric effects in three-dimensional spatially developing mixing layers. In *Proc. Seventh Symp. on Turbulent Shear Flows, Stanford University*, pp. 9.2.1–9.2.6.

Champagne, F. H. 1978 The fine-scale structure of the turbulent velocity field. *J. Fluid Mech.* **86**, 67–108.

Chandrsuda, C., Mehta, R. D., Weir, A. D. & Bradshaw, P. 1978 Effect of free-stream turbulence on large structures in turbulent mixing layers. *J. Fluid Mech.* **85**, 693–704.

Corcos, G. M. 1988 The role of cartoons in turbulence. In *Perspectives in Fluid Mechanics* (ed. D. E. Coles). Lecture Notes in Physics, vol. 320, pp. 48–65. Springer.

Corcos, G. M. & Lin, S J. 1984 The mixing layer: deterministic models of a turbulent flow. Part 2. The origin of the three-dimensional motion. *J. Fluid Mech.* **139**, 67–95.

Fiedler, H. E. 1988 Coherent structures in turbulent flows. *Prog. Aerospace Sci.* **25**, 231–269.

Fiedler, H. E., Glezer, A. & Wygnanski, I. J. 1988 Control of the plane mixing layer: some novel experiments. In *Current Trends in Turbulence Research* (ed. H. Branover, M. Mond & Y. Unger), vol. 112, pp. 30–64.

Fiedler, H. E., Nottmeyer, K., Wegener, P. P. & Raghu, S. 1985 Schlieren photography of water flow. *Exps Fluids* **3**, 145–151.

Gaster, M., Kit, E. & Wygnanski, I. J. 1985 Large scale structures in a forced turbulent mixing layer. *J. Fluid Mech.* **150**, 23–47.

Glezer, A. & Coles, D. E. 1990 An experimental investigation of a turbulent vortex ring. *J. Fluid Mech.* **211**, 243–283.

Glezer, A., Katz, Y. & Wygnanski, I. J. 1989 On the breakdown of the wave packet trailing a turbulent spot in a laminar boundary layer. *J. Fluid Mech.* **198**, 1–26.

Ho, C.-M. & Huerre, P. 1984 Perturbed free shear layers. *Ann. Rev. Fluid Mech.* **16**, 365–424.

Huang, L.-S. & Ho, C.-M. 1990 Small-scale transition in a plane mixing layer. *J. Fluid Mech.* **210**, 475–500.

Hussain, A. K. M. F. 1983 Coherent structures and incoherent turbulence. In *Turbulence and Chaotic Phenomena in Fluids: Proc. Intl Symp. on Turbulence and Chaotic Phenomena in Fluids, Kyoto, Japan* (ed. T. Tatsumi). Elsevier.

Jimenez, J. 1983 A spanwise structure in the plane shear layer. *J. Fluid Mech.* **132**, 319–336.

Jimenez, J., Martinez-Val, R. & Rebollo, M. 1979 On the origin and evolution of three-dimensional effects in the mixing layer. *Final Rep.* DA-ERO 79-G-079. Universidad Politecnica de Madrid. AD-A096007.

Klebanoff, P. S., Tidstrom, K. D. & Sargent, L. M. 1962 The three-dimensional nature of boundary layer instability. *J. Fluid Mech.* **12**, 1–41.

Konrad, J. H. 1976 An experimental investigation of mixing in two-dimensional turbulent shear flows with applications to diffusion limited chemical reactions. Ph.D. thesis, California Institute of Technology.

Landahl, M. T. & Mollo-Christensen, E. 1986 *Turbulence and Random Processes in Fluid Mechanics.* Cambridge University Press.

LASHERAS, J. S. & CHOI, H. 1988 Three-dimensional instability of a plane free shear layer: an experimental study of the formation and evolution of streamwise vortices. *J. Fluid Mech.* **189**, 53–86.

LASHERAS, J. C., CHO, J. S. & MAXWORTHY, T. 1986 On the origin and evolution of streamwise vortical structures in a plane, free shear layer. *J. Fluid Mech.* **172**, 231–258.

LEIBOVICH, S. 1983 The form and dynamics of Langmuir circulations. *Ann. Rev. Fluid Mech.* **15**, 391–427.

LIEPMANN, H. W., BROWN, G. L. & NOSENCHUCK, D. M. 1982 Control of laminar instability-waves using a new technique. *J. Fluid Mech.* **118**, 187–200.

LIN, S. J. & CORCOS, G. M. 1984 The mixing layer: deterministic model of a turbulent flow. Part 3. The effect of plane strain on the dynamics of streamwise vortices. *J. Fluid Mech.* **141**, 139–178.

METCALFE, R. W., ORSZAG, S. A., BRACHET, M. E., MENON, S. & RILEY, J. J. 1987 Secondary instability of a temporally growing mixing layer. *J. Fluid Mech.* **184**, 207–243.

MIKSAD, R. W. 1972 Experiments on the nonlinear stages of free-shear-layer transition. *J. Fluid Mech.* **56**, 695–719.

NYGAARD, K. J. 1987 Construction, instrumentation, and testing of a spanwise forced plane mixing layer facility. M.S. Report, The University of Arizona.

NYGAARD, K. J. & GLEZER, A. 1989 On the spanwise structure of a plane mixing layer. In *Advances in Turbulence 2* (ed. H.-H. Fernholtz & H. E. Fiedler), pp. 461–466. Springer.

NYGAARD, K. J. & GLEZER, A. 1990 Core instability of the spanwise vortices in a plane mixing layer. *Phys. Fluids* A **2**, 461–464.

NYGAARD, K. J. & GLEZER, A. 1991 Phase excitation of a plane mixing layer. *J. Fluid Mech.* (to be submitted).

OSTER, D. & WYGNANSKI, I. 1982 The forced mixing layer between parallel stream. *J. Fluid Mech.* **123**, 91–130.

PIERREHUMBERT, R. T. 1986 Universal short-wave instability of two-dimensional eddies in an inviscid fluid. *Phys. Rev. Lett.* **57**, 2157–2159.

PIERREHUMBERT, R. T. & WIDNALL, S. E. 1982 The two- and three-dimensional instabilities of a spatially periodic shear layer. *J. Fluid Mech.* **114**, 59–82.

PULLIN, D. I. & JACOBS, P. A. 1986 Inviscid evolution of stretched vortex arrays. *J. Fluid Mech.* **171**, 377–406.

RILEY, J. J., MOURAD, P. D., MOSER, R. D. & ROGERS, M. M. 1988 Sensitivity of mixing layers to three-dimensional forcing. In *Center for Turbulence Research: Proc. Summer Program 1988*, pp. 91–116. Center for Turbulence Research.

ROBERTS,. F. A. 1985 Effects of a periodic disturbance on structure and mixing in turbulent shear layers and wakes. Ph.D. thesis, California Institute of Technology.

ROGERS, M. M. & MOSER, R. D. 1989 The development of three-dimensional temporally evolving mixing layers. In *Proc. Seventh Symp. on Turbulent Shear Flows, Stanford University*, pp. 9.3.1.–9.3.6.

ROSHKO, A. 1981 The plane mixing layer; flow visualization results and three-dimensional effects. In *The Role of Coherent Structures in Modelling Turbulence and Mixing* (ed. J. Jimenez). Lecture Notes in Physics, vol. 136, pp. 208–217. Springer.

SARIC, W. S. & THOMAS, A. S. W. 1983 Experiments on the subharmonic routes to turbulence in boundary layers. In *Turbulence and Chaotic Phenomena in Fluids: Proc. Intl Symp. on Turbulence and Chaotic Phenomena in Fluids, Kyoto, Japan* (ed. T. Tatsumi). Elsevier.

SCHLICHTING, H. 1968 *Boundary Layer Theory*. McGraw-Hill.

TOWNSEND, A. A. 1980 *The Structure of Turbulent Shear Flows*, 2nd edn. Cambridge University Press.

WEISBROT, I. 1984 A highly excited turbulent mixing layer. M.S. thesis Tel Aviv University.